HELSINKI UNIVERSITY OF TECHNOLOGY
Department of Electrical and Communications Engineering
Laboratory of Computational Engineering

Kim Pihlström

A Monte Carlo Study of Two-Dimensional Nanodroplet Dynamics

Master's Thesis
Laboratory of Computational Engineering

Supervisor: Professor Kimmo Kaski
Instructor: Dr. Riku Linna

Espoo November 30, 2007

TEKNILLINEN KORKEAKOULU
HELSINKI UNIVERSITY OF TECHNOLOGY

Helsinki University of Technology
Laboratory of Computational Engineering
Innopoli 2, Tekniikantie 14
P.O.Box 9203
FI-02015 TKK
FINLAND
Tel. +358 9 451 5726
Fax. +358 9 451 4833
http://www.lce.hut.fi

E-mail: kim.pihlstrom@tkk.fi

HELSINKI UNIVERSITY OF TECHNOLOGY
Department of Electrical and Communications Engineering
Master's Programme of Electronics and Electrical Engineering

ABSTRACT OF MASTER'S THESIS

Author: Kim Pihlström

Title of thesis:
A Monte Carlo Study of Two-Dimensional Nanodroplet Dynamics

Date: November 30, 2007 **Pages:** 17 + 74
Professorship: Computational Engineering **Code:** S-114
Supervisor: Professor Kimmo Kaski
Instructor: Dr. Riku Linna

This thesis discusses the dynamics of droplet translocation on lattices with potential gradient steps. Due to recent developments in manipulating droplets of a few nano-litres understanding the dynamics of nano-scale droplets has become important.

The model used in this study consists of an Ising system simulated using the N-fold way method at very low temperatures. For creating new trial configurations we use Kawasaki dynamics. The potential gradients act over straight edges translocating droplets. Other geometries for the potentials producing unexpected results are also presented. When studying the droplet translocation over a potential we record the centre-of-mass location as well as modes of motion. The modes of motion describe how single particles move. Systems where the droplet is periodically connected in the direction of the step edge are used as a reference and to validate the model. The actual system investigated in this thesis is a two-dimensional free droplet driven by varying potentials on a solid surface. In order to characterise the dimensional behaviour of the free droplet, we perform a finite-size scaling and are able to achieve a data collapse when varying the field and dimensions of the droplet.

The motivation for studying this system is to gain a better understanding of how droplets translocate over a step edge and to determine the necessary conditions for the ballistic translocation of a droplet on a surface.

Keywords: Nanodroplet, Monte Carlo, N-fold way, Ising, lattice gas, finite size scaling, driven diffusion
Language: English

TEKNISKA HÖGSKOLAN
Avdelningen för el och telekommunikationsteknik
Utbildningsprogrammet för elektronik och elektroteknik

SAMMANDRAG AV
DIPLOMARBETET

Utfört av: Kim Pihlström

Arbetets namn:
Monte Carlo studie av tvådimensionell nanodroppe dynamik

Datum: 30 november 2007 **Sidoantal:** 17 + 74
Professur: Datorbaserad teknik **Kod:** S-114
Övervakare: prof. Kimmo Kaski
Handledare: Dr. Riku Linna

Detta examensarbete handlar om dynamiken hos droppar som rör sig över en yta med potentialsteg. Det har blivit allt viktigare att förstå dynamiken hos nanodroppar eftersom färska forskningsresultat har visat att det är möjligt att manipulera droppar så små som ett fåtal nanoliter.

Modellen som används i denna studie simuleras vid väldigt låga temperaturer m.h.a. ett Ising system som uppdateras av "N-fold way" metoden. För att skapa nya konfigurationer använder vi oss av Kawasaki dynamik. Potentialens gradient har en stegliknande form som förflyttar droppen. Andra geometrier för potentialens form har också undersökts från vilka förvånande resultat presenteras. Vi beräknar droppens massmedelpunkt såväl som dess rörelsesätt då den rör sig över en potential. Rörelsesätten beskriver hur enskilda partiklar rör sig. System där droppen är periodiskt länkad i samma riktning som potentialstegen har använts som referens samt för att bekräfta att modellen fungerar. Det egentliga systemet som studeras i detta examensarbete är en tvådimensionell droppe, som inte är periodiskt länkad, vilken drivs av varierande potentialer på en fast yta. Vi genomför en "finite-size scaling" och åstadkommer en data kollaps, då vi varierar fältet och droppens dimensioner, för att kunna karakterisera den icke periodiskt länkade droppens dimensionella beteende.

Vi har studerat detta system för att bättre förstå hur droppar rör sig över potentialsteg samt för att fastställa vilka villkor som bör uppfyllas för att droppen skall röra sig ballistiskt över en yta.

Nyckelord: Nanodroppe, Monte Carlo, N-fold way, Ising, lattice gas, finite-size scaling, driven diffusion
Språk: Engelska

Acknowledgements

The research presented in this thesis has been carried out in the Laboratory of Computational Engineering (LCE) at Helsinki University of Technology (HUT), during the years 2005-2007. This project was started in the summer of 2005, under the supervision of Dr. Alex Bunker. During the autumn of 2005, Dr. Riku Linna overtook supervision.

My thanks go to Professor Kimmo Kaski for giving me the opportunity to combine the research work with my studies. I also would like to thank Dr. Riku Linna for his guidance and support while writing this thesis and for the many fruitful discussions we had while working on this project.

I would like to thank all of my coworkers at LCE for providing a pleasant working environment as well as all my friends for their support and optimism towards my studies.

Finally, my deepest thanks go to my parents for providing their support throughout my student days.

Espoo November 30, 2007

Kim Pihlström

Abbreviations and Acronyms

Monte Carlo	A simulation that relies heavily on random number or quarter in Monaco.
2D-Ising model	A model that consists of a 2-dimensional lattice filled with spins which can have one of two values, or for lattice gas systems spins are referred to as particles and holes. The total energy of the system follows a well known Hamiltonian.
Kawasaki dynamics	A method for flipping the spins on the simulation lattice. This method conserves the total number of spin, or for a lattice gas it conserves the total number of particles. This method is what is known as a time driven method.
N-fold way	A method that flips spins by choosing events based on their probability to occur. This method is known as a event driven method.
Drop or droplet	Collection of particles that form an island. The shape of the drop is created to be square, size $L_x \times L_y$, in its initial configuration.
Step or surface	Means a surface that a particle can move around on without changing its energy.
Step edge or grain boundary	Refers to the edge of a surface. When a particle makes a move over this edge its energy will change.
Modes of movement	Several modes are identified for how a particle can move on a surface. These modes are distinguished by counting the number of neighbors a particle has before and after it has been moved.
Periodic system	Is a system where the width of the lattice is the same the width of the drop being simulated on it. The drop in a periodic system is refered to as a periodic drop.
Non-periodic system	The drop width is smaller than the width of the lattice. The drop in this system is refered to as a free drop.

Contents

List of Figures

List of Tables

Chapter 1

Introduction

1.1 The setup

In this thesis the phenomenon where a nanoscale droplet moves over a surface with a potential gradient is studied.

The droplet is made out of a 2 dimensional layer of particles placed on a square lattice. The maximum size of the droplet is only a few thousand particles, so the system is microscopic. The droplet is placed on a surface that contains a step-like potential over which it is then allowed to move freely. The potential drops by Δh at every position interval Δx. A particle interacts with its nearest neighbours and with the field created by the surface.

To give an idea of what the setup looks like, a picture of a typical system is shown in Fig. 1.1. The height of the steps in this picture is proportional to the energy contribution the particles get from interacting with the surface. The lower the steps are, the lower is the potential difference. The rest of the energy comes from nearest neighbour interactions with the four nearest particles.

Initially, it was expected that the droplet would move in one out of two ways. It would either move by what is known as driven diffusion or by ballistic motion. Indeed, these two ways of moving were seen in the simulations. Driven diffusion means that the particles do not move only by randomly diffusing about, but instead single particles see the direction in which the potential decreases as more probable and therefore on average tend to move

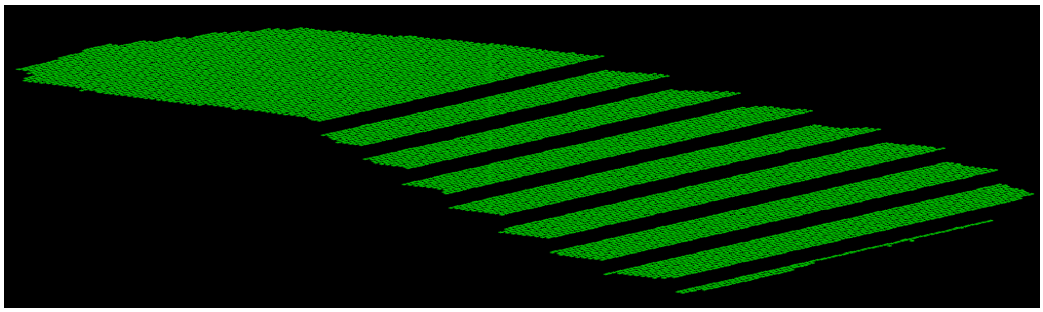

Figure 1.1: A side view of a configuration that shows the change in the field as a function of height. The higher the particles are located in the picture the stronger is the field that acts on them.

in that direction. Ballistic motion occurs when the entire droplet moves, without breaking up considerably, down the steps. Driven diffusion becomes more probable as the field difference between two steps is increased or when the length of a step is increased.

In the following chapter we will present some previous work done in this field and also discuss what the most important aspects have been in the study of droplets. M. Voué *et al.* review in their article [1] what has been done in recent years: the methods that have been used and the most important results.

1.2 Previous work

There have been related studies in the past. Recent developments in the process of forming and actuating droplets as small as a few nano-litres, see [2], have made it increasingly important to understand the dynamics of nano-scale droplets. An important phenomenon concerning droplets is how they spread on surfaces. Accordingly, a lot of theoretical and computational effort has been devoted to understanding the spreading of very small droplets, for which the classical Young's equation may fail [3].

There have not been many studies in the past that focus on studying the effect a heterogeneous surface has on the morphology of a droplet, despite important practical applications, such as the so called lab-on-a-chip. There are a few studies on this subject, however. For example in [4] a droplet is studied on a chemically striped (lyophobic-lyophilic) surface. Another such study is the one performed by Yeomans, Kusumaatmaja, *et al.* [5]. The

biggest differences in their study compared to the present study is that they used a more lattice Boltzmann model, to simulate a macroscopic droplet on a surface with a groove, whereas we simulate a nano-scale droplet on surfaces with one or multiple steps. Another significant difference is that in order for Yeomans, Kusumaatmaja, *et al.* to observe motion they had to give the droplet an initial velocity, whereas this is not needed in our model. The capillary forces that are driving the droplet over the surface in the lattice Boltzmann study are not the reason for the ballistic motion of a droplet over the surface observed in this study. When studying a droplet at a micro- or nanoscopic scale other mechanisms are responsible for moving the droplet over the surface.

There have for a long time been a need to understand how liquid wets surfaces. For example, it is important to know how ink spreads on a paper or how lubrication behaves on surfaces found in engines. For a review on how friction works on a nanoscale see [6]. To be able to design materials that are optimal for their given purpose we need to know how they work on a microscopic scale. For example in [7, 8, 9] droplets are being studied on homogeneous surfaces using various techniques.

Other studies involving droplets focus on studying the precursor film that is forming in the vicinity of the droplet as it approaches equilibrium [10, 11, 12], terraced spreading of monomolecular layers [13, 14, 15, 16] and viscous losses due to rolling motion [17, 18].

Using molecular dynamics it was found by Yang, Koplik and Banavar [8, 19] that the radius of the layers spread as $R \sim \sqrt{\log(t)}$ when studying spreading of droplets in the terraced wetting regime. This result differs from the experimental and simulated observations in [9, 14, 20, 15, 21, 22]. The model used by J. De Coninck, *et al.* [9] performs Kawasaki dynamics for a lattice gas which reproduces the same time dependence for the growth of layers as was observed from experiments, $R \sim \sqrt{t}$, where t is time. The radius of the precursor film was measured experimentally using refined ellipsometry. The difference between Banavar's, *et al.*, results and those presented above is believed to come from the difference in molecular size between the experiments and the simulations [9]. Later it was suggested by Nieminen *et al.* [7] that in Yang, Koplik and Banavar's [19] model molecules evaporate from the droplet and wet the surface of the solid whereas in [9] the droplet used in the experiments is much less volatile.

This same spreading law was even found by using a macroscopic model to simulate particles diffusing about on a lattice [23]. In this study S. F. Burlatsky, *et al.* were able to reproduce the spreading law by using small metallic balls

(both magnetic and non-magnetic balls were used, though in separate experiments) placed on a vibrating lattice. The lattice is made to vibrate by having two motors placed at each end of the lattice. These motors are fitted with eccentrical flywheels to provide the random motion for the balls. In their report they show that this system indeed produces diffusive motion.

Using Monte Carlo simulations D. B. Abraham, *et al.* [24] were able to reproduce the same time dependence of the radius of the spreading precursor film as was experimentally observed in other studies.

The first description of a molecular film preceding the droplet was done by Hardy in 1919 [25].

The case where a one layer thick precursor film is spreading before the droplet can be observed when, for example, the temperature is raised and the contact angle between the droplet and the substrate reaches zero. Experimental work on wetting has been done by Young and Laplace [10].

In a recent study, a macroscopic drop was studied on a vibrating inclined surface [26]. The surprising finding in this study is how the drop is able to move in the opposite direction to which gravity would move it, if the surface was not be vibrating.

The systems studied in this thesis can be related to these monolayer films and terraced layers by the fact that we are looking at one atom layer thick films here also.

In this thesis droplets will be studied on a surface with a step-like potential using Monte Carlo simulations.

1.3 The model

To model the system a 2D Ising Monte Carlo simulation is constructed. Instead of using the more common Metropolis algorithm for doing the individual updates on the simulated lattice, the more exotic N-fold way algorithm is used [27]. The reason for using the N-fold way instead of the Metropolis algorithm is due to our observation that the ballistic motion occurs only at very low temperatures. At low temperatures the Metropolis algorithm is very slow, whereas the N-fold way algorithm is much faster due to the fact that it is a so called event driven algorithm. The Metropolis algorithm is what is known as a time step driven algorithm. The difference between a time step driven and an event driven algorithm is that in the former during each new iteration of the algorithm a move occurs only with some probability, whereas

in an event driven algorithm something always happens during every iteration. In the case of the N-fold way algorithm an update is selected to occur at every attempt. The update is selected based on how probable it would be to occur in the Metropolis algorithm.

The N-fold way algorithm may look like a very powerful and fast algorithm at a first glance but in reality this is not always the case. The N-fold way algorithm is faster than the Metropolis algorithm only at low temperatures. The reason for this is that a lot of bookkeeping is necessary in the N-fold way algorithm. Unlike the Metropolis algorithm, the N-fold way algorithm must keep track of all the possible moves and their probabilities.

In Section 3.11 we compare the Metroplis method to the N-fold way method. Using those simulations we calculate the time scaling factor, τ, in used in the N-fold way method. We also calculate how much faster the N-fold way method is compared to the Metropolis method when simulating the same kind of systems as we study in this thesis.

Kawasaki dynamics is chosen to handle the creation of new trial configurations, since it preserves the number of particles in the simulation. The methods and algorithms described here will be presented a second time in Section 2, where they will also be described in more detail.

For studying the systems only a few parameters are varied. The most important parameters are the temperature, T, the step length, Δx, and the drop in the potential, Δh, as a particle moves over a step. In addition, other quite important parameters are the size of the droplet, its location, and the size of the system. In most of the simulations only the total drop in potential between the first and the last step, the initial distance of the droplet from the first step and the number of steps between the first and last step are changed. The rest of the parameters are kept constant.

An example of a physical system that could be simulated using the model described above is a layer of particles, which has been deposited on the surface of some substrate having chemically fabricated stripes. The stripes function as a potential that the particle layer interacts with.

1.4 Applications

The reason for studying nano-scale droplets is because knowing how droplets behave on surfaces with varying textures is very important to fully understand how a number of different technologies such as lubrication, painting,

coating, emulsion, dying, gluing and oil recovery from porous rocks work [10, 28, 29, 30, 31].

In reality, a system with a step like potential could be used in droplet filters or as a way of transporting a molecule over some surface, on which it normally does not favour moving. After a number of simulations it was clear that the steps cannot be arbitrarily long, since the time needed for the droplet to find the next step grows with the distance from the edge of a lower step. When a droplet moves over a step it needs to find the edge of the next step before it can proceed to move further down the steps. If the droplet is small enough, it will take a considerable time before it finds the next step. As long as the droplet is located on a single step, only diffusion will be moving it around. In other words, the droplet will be moving around on the step randomly until it finds an energetically more favourable step to move onto. Based on this fact, a filter could be constructed such that the length of the steps is chosen so that only droplets larger than some critical size will proceed to the next step. Results from simulations studying a filter-like setup are presented in Section 3.7.

A molecular transportation system could work by attaching a molecule on the droplet and then letting the droplet be driven over a surface which has chemically fabricated stripes etched on it. By modifying the surface one could then create a transport mechanism for molecules.

This study mainly focuses on investigating the effect a single step or two steps have on droplets varying in size from 50 particles 40000 particles.

In Section 3.10 we study an alternative geometry of the step edge in hope of finding a way to further increase the stability and velocity of the droplet as it translocates. The field we study is shaped like a triangle that opens in the direction in which the droplet is moving. We find in this section that we are able to increase the droplet's velocity without it breaking up.

In the next chapters results will be presented from studies with a droplet moving over one step. The dominating modes at different parameter configurations were identified. As a result, it was found that the number of particles moving along the edges of the droplet will grow with respect to particles moving inside the droplet as the field parameter is decreased, or in other words, the step height is lowered. Then, a second step was added to study in what way the droplet moved over them and also to check, whether it moved in the same way as it did when moving over the first step edge.

Chapter 2

Methods

2.1 Monte Carlo method

In the previous chapter we mentioned that we constructed a Monte Carlo model for studying the movement of a nanoscale droplet across a surface with a potential gradient.

A Monte Carlo algorithm relies heavily on random numbers. The name Monte Carlo for simulations like those performed in this study, refers to the random behaviour exhibited by many games played in the numerous casinos in a quarter, in Monaco, with the same name.

There are numerous books written on the subject of Monte Carlo methods. The two books about Monte Carlo simulations used in this study are by D. Landau & K .Binder [32] and M. E. J. Newman & G. T. Barkema [33].

Before the real problem, or the algorithms used for solving it, will be discussed any further, a few examples will be given to give better insight on how Monte Carlo methods, or random numbers, can be used to solve simple problems.

One easy and sometimes handy use of computers is for numerical solution of analytically difficult, or unsolvable, integrals. The easiest case is when we have a one-dimensional integral of the form

$$I = \int_b^a f(x)dx.$$

There exists several numerical methods for solving a problem like this, for example trapezoidal rule or Simpson's rule. In the next section we will describe the so-called hit-or-miss method to demonstrate the Monte Carlo computation. Later, also more sophisticated methods will be presented.

2.1.1 Hit-or-miss method

The hit-or-miss method is a rather unsophisticated, brute force way of using computers to evaluate an integral. The idea for the hit-or-miss method is simple. We start by drawing a box around a function $f(x)$ in the interval $[a, b]$. The bottom side of the box extends from a to b, the other sides extend from 0 to f_{max}, where f_{max} is the maximum value $f(x)$ can have when $x \in [a, b]$.

Next, we start filling this box with N randomly selected points, or pairs of random numbers. Once N points have been added to the box we count how many of these N points are below the graph $f(x)$. The value of the integral can then be easily estimated using the formula

$$I_{est} = \frac{N_{under}}{N} A,$$

where N_{under} refers to the number of points under $f(x)$. The area A is the area of the box that was previously drawn around the interval of integration, in other words $A = f_{max} |b - a|$.

By increasing the amount of random numbers that we used for evaluating the integral we can decrease the error in the estimate. In other words, as $N \to \infty$ the estimated integral value will eventually converge to the correct value.

Since the method presented here was based on random events, we will also want to know how large an error we make when estimating an integral this way. Therefore, in order to obtain also an error estimate, the algorithm is usually repeated several times, using different random number series in each iteration. From these iterations the standard deviation can be calculated to give an estimate of the validity of the obtained results.

The hit-or-miss method works well as long as the integrand is fairly smooth. If the integrand varies a lot, like the function in Fig. 2.1 does near origin, we will need a lot more random points to obtain a result with at least equal precision to the one obtained for a smooth function.

In the case of a rapidly varying integrand, greater errors in the estimate can be expected and usually many more random points are needed to produce an estimate of equal precision for it than for a smoother integrand.

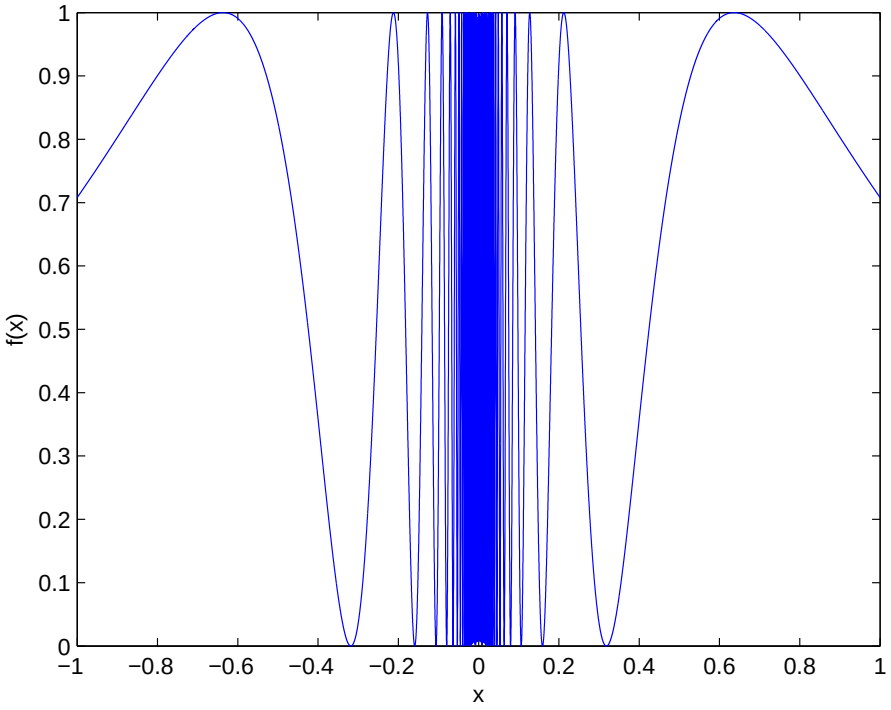

Figure 2.1: Plot of $f(x) = \sin^2\left(\frac{1}{x}\right)$.

2.1.2 Importance sampling

The hit-or-miss method works well when the function to be integrated is fairly smooth and we can use a large amount of random numbers.

A more intelligent method for numerical integration is the importance sampling method. The advantage of importance sampling, over the hit-or-miss method with the same number of random points is the higher precision. The drawback is that the importance sampling method requires *a priori* knowledge about the integrand, in other words, we need to know which regions of the integrand will cause the hit-or-miss method to behave badly.

The idea with the importance sampling method is that we first identify regions where the integrand will generate a large error contribution. Then we choose a weight function, $w(x)$, which ensures that these badly behaving regions receive more random numbers than the other, smooth parts of the integrand. Finally, when we calculate the integral we have to factor in the

weight function to obtain the correct value.

The weight function is a positive normalised function, in other words

$$\int_a^b w(x)dx = 1.$$

This requirement on the weight function ensures that the random points are all generated inside the desired interval $[a, b]$.

The idea with the weight function is that it gives more emphasis on regions, where the integrand behaves badly by generating more random numbers in these regions. We can now write the integral in the following form

$$I = \int_a^b \left[\frac{f(x)}{w(x)}\right] w(x)dx.$$

The estimate is now given by

$$I_{est} = \frac{1}{N}\sum_{i=1}^{N} \frac{f(x_i)}{w(x_i)},$$

where the points x_i are generated according to the weight function $w(x)$. It is a good idea to choose $w(x)$ to mimic the integrand. That way the quotient $\frac{f(x)}{w(x)}$ is slowly varying, and the error contribution is reduced.

2.2 The two dimensional Ising model

The Ising model [32] is one of the simplest models one can use to study physical systems. The two dimensional Ising model is a well known problem in statistical mechanics, studied for quite some time. By using well established techniques of mathematical physics it can even be solved exactly [34, 35, 36].

The two dimensional Ising model can consist of a square lattice of size $L \times L$, where each site can have one out of two values, for example -1 and 1 in magnetic systems. The lattice is then populated with spins (or particles, depending on what kind of environment is being simulated) that can interact at the same time with their nearest-neighbour interactions and with an external potential.

If the lattice is populated with particles, the system is referred to as an Ising lattice gas. This systems is equivalent to a normal Ising system that uses 1

and -1 to represent a spin up and spin down, respectively. In the lattice gas model we use in this thesis we use 1 and -1 to represent empty sites and a filled sites, respectively. The system that can be studied with this model are very different from those addressed by the conventional Ising model.

The lattice gas model is a conserved-order-parameter, or COP, Ising model [33]. The order parameter in an Ising simulation is the magnetisation, $\langle M \rangle = \langle \sum_i^N s_i \rangle$, or mean magnetisation per spin $\langle m \rangle = \frac{1}{N} \langle \sum_i^N s_i \rangle$. Conserved-order-parameter means the magnetisation is kept constant, so the total number of spins or, in the case of lattice gas systems, the number particles is constant throughout the simulations.

The Hamiltonian for the Ising model is given by

$$\mathcal{H} = -\mathbf{J} \sum_{\langle i,j \rangle} s_i s_j - \mathbf{H} \sum_i s_i, \tag{2.1}$$

where the first term is a sum taken only over all nearest-neighbour pairs and the second term is a sum over all particles (or spins) in the system. In other words, the first sum in the Hamiltonian is the energy contribution that comes from particles interacting with neighbouring particles and the second sum is the energy contribution that comes when individual spins interact with the external potential. In this study the external potential is used to model the surface that droplet is thought to move on. The parameter $\mathbf{J}$ is a coupling constant between nearest-neighbour pairs and $\mathbf{H}$ is the magnitude of the external field. In the Hamiltonian above, the field parameter, $\mathbf{H}$, is assumed to be independent of the location of the spin, in other words, it is assumed to be a constant throughout the whole system.

In the case of the system studied in this thesis, where the external field depends on the x- and y-coordinates of the particle, the field parameter is moved inside the second sum in Eq. (2.1) and is now denoted as $\mathbf{H}(x, y)$ to make its x and y dependence explicit.

$$\mathcal{H} = -\mathbf{J} \sum_{\langle i,j \rangle} s_i s_j - \sum_i \mathbf{H}[x(s_i), y(s_i)] s_i. \tag{2.2}$$

Here, $x(s_i)$ and $y(s_i)$ are functions that extract the x- and y- coordinates from the spin s_i. When studying the system described in Chapter 1 we have a Hamiltonian that depends only on the y-coordinate, in other words, we can forget the $x(s_i)$ parameter and write $\mathbf{H}(y(s_i))$.

Below the critical temperature, T_c, systems with a conserved-order-parameter will undergo a phase separation and arrange themselves into local domains

[33]. These local domains will have either of the two preferred densities, ρ_+ and ρ_-. Normal Ising systems with temperatures below T_c have been found to have either one of these densities in their equilibrium configuration. ρ_+ and ρ_- are found to be

$$\rho_+ = \frac{1}{2}\left(1 + |m|\right), \qquad \rho_- = \frac{1}{2}\left(1 - |m|\right). \tag{2.3}$$

They are derived from $\sum_i^N s_i = \frac{1}{2}\left(\frac{M}{N} + 1\right)$, where $\sum_i^N s_i$ is the sum over all lattice sites, $N = L_x \times L_y$, and s_i can be either $s_- = -1$ or $s_+ = 1$. On a lattice where the lattice sites can take the values $\sigma_+ = 1$ or $\sigma_- = 0$ we have equivalently $\sum_i^N \sigma_i = \rho N$. Eq. (2.3) are derived by noticing that $\sigma_i = \frac{1}{2}\left(s_i + 1\right)$ and that for the normal Ising model the average magnetisation, $m = \frac{M}{N}$, has two equilibrium values, one negative and one positive. These two densities are temperature dependent: the lower the temperature, the closer to $\rho_+ = 1$ and $\rho_- = 0$ will the system's density get.

From this we get the area in the phase diagram to the left of the critical temperature in Fig. 2.2. ρ_+ and ρ_- approach each other as the temperature approaches T_c. Above the critical temperature ρ_+ and ρ_- are equal.

If the density, ρ, for the COP system is picked to be inside the range $[\rho_-, \rho_+]$ then the system will arrange itself to obtain local domains with either ρ_+ or ρ_-. ρ_+ and ρ_- will be very close to zero and one, respectively, for most simulations presented later in the thesis. In other words, there will be a clear interface between these domains. This is due to all simulations being performed at very low temperatures. Above the critical temperature the system is homogeneous.

2.3 The Metropolis Algorithm

The Metropolis algorithm generates a new configuration from a previous configuration with a certain probability, p. The probability with which the new configuration will be accepted is dependent only on the energy difference between these two states. The probability of going from one configuration to another is given by the following equation

$$w_{ij} = \begin{cases} e^{-\Delta E/k_B T} & \text{if} \quad \Delta E > 0 \\ 1 & \text{if} \quad \Delta E \leq 0, \end{cases} \tag{2.4}$$

where ΔE is the energy difference between two successive states, $\Delta E =$

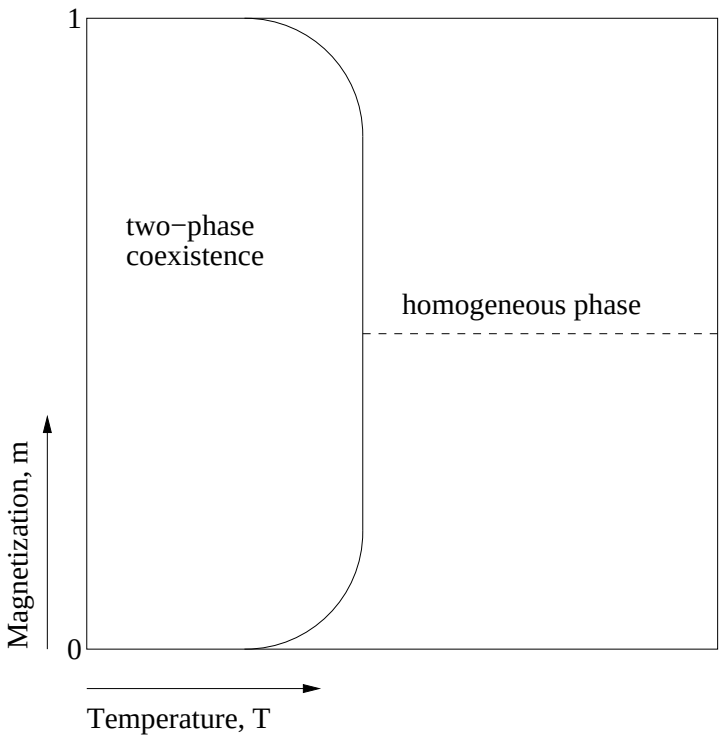

Figure 2.2: Phase diagram of the two dimensional COP Ising model. The system will separate into coexisting domains below the critical temperature, T_c. Above T_c the system will be homogeneous.

$E_{i+1} - E_i$. In the case when the energy of the new trial configuration is lower than that of the last accepted configuration the Metropolis algorithm has created, the trial configuration will be automatically accepted as the current configuration for the system. Since Eq. (2.4) is very important, its derivation is given next.

Eq. (2.4) is obtained from what is known as the Master equation for a Markov chain. A Markov chain is a stochastic process in which random variables, r_i, depend only on the preceding variable, r_{i-1}. In other words, a Markov chain has no memory. Mathematically, a Markov chain can be expressed as

$$p(r_{i+1}|r_i r_{i-1} \dots r_1) = p(r_{i+1}|r_i), \tag{2.5}$$

where $p_i(t) = p(r_i, t)$ is the probability of finding the system in state i at time t. The Master equation, given by

$$\frac{\partial p_i(t)}{\partial t} = -\sum_{j=1}^{N} \left[w_{ij} p_i - w_{ji} p_j \right], \tag{2.6}$$

is a direct consequence of the Markov chain in Eq. (2.5). w_{ij} is the transition rate for a system going from state i to state j. The Master equation can be interpreted so that the "flow of probability" between two states in a Markov chain is equal. When the system is in equilibrium, the net flow of probability in and out of a state in the chain is zero,

$$\frac{\partial p_i(t)}{\partial t} = 0. \tag{2.7}$$

Plugging this into Eq. (2.6) gives

$$w_{ij} p_i = w_{ji} p_j \quad \Rightarrow \quad \frac{w_{ij}}{w_{ji}} = \frac{p_j}{p_i}. \tag{2.8}$$

For a classical canonical ensemble,

$$p_i = \frac{1}{Z} e^{-E_i/k_B T} \tag{2.9}$$

gives the probability that the ith state will occur, Z is the partition function and is given by

$$Z = \sum_{i}^{N} e^{-E_i/k_B T}, \tag{2.10}$$

assuming there are N different states in the ensemble.

The probability in Eq. (2.9) usually cannot be calculated directly since for most systems Z is impossible to determine. The main advantage of the Metropolis algorithm is that one needs not have exact knowledge of Z at all times.

When Eq. (2.9) is substituted into Eq. (2.8), one gets

$$\frac{w_{ij}}{w_{ji}} = \frac{p_j}{p_i} = \frac{\frac{1}{Z} e^{-E_j/k_B T}}{\frac{1}{Z} e^{-E_i/k_B T}} = e^{(E_i - E_j)/k_B T} = e^{-\Delta E/k_B T}, \tag{2.11}$$

where ΔE is the change in energy from the previous state to the current state, i.e. $\Delta E = E_j - E_i$.

Using the result above, we are now in a position to solve for the probability of a system to go from one configuration to another. The result we obtain is the same that was originally presented in Eq. (2.4) when $\Delta E > 0$. A convenient choice is to accept all transitions where the energy decreases in the system, $\Delta E \leq 0$.

$$p_{i\to j} = \begin{cases} e^{-\Delta E/k_B T} & \text{if} \quad \Delta E > 0 \\ 1 & \text{if} \quad \Delta E \leq 0. \end{cases} \tag{2.12}$$

The algorithm described above is a time-step driven algorithm: an update can be either accepted or rejected during each iteration.

When an update on the lattice has been made, the corresponding energy change, ΔE, is calculated. If $\Delta E \leq 0$, the update is accepted but if $\Delta E > 0$, a new random number is chosen and ΔE is inserted into Eq. (2.4). If the random number is smaller than the value obtained from inserting ΔE into Eq. (2.4), the move is accepted.

From the way the probability for the acceptance of a new configuration is calculated, it can be seen that this time-step driven update algorithm works very well at high enough a temperature (when the temperature is high, then the probability is high for a move to occur). However, longer and longer runs are needed when the temperature is lowered due to the Boltzmann weight in Eq. (2.12). As the temperature is lowered, the probability for a system to go from state i to state j also gets lower. A more efficient update algorithm at low temperatures, known as the N-fold way, will be discussed in Section 2.4. The N-fold way algorithm is an event driven update algorithm. Thus, even at very low temperatures, an update happens at every iteration.

There are several methods for generating new trial configurations. The one known as Kawasaki dynamics will be presented in Section 2.5. This method can be easily adapted to simulations where particles are used. Other methods for generating new trial configurations are better suited for simulations where, for example, magnetisation is studied.

2.4 N-fold way update scheme

At low temperatures the N-fold way, an event-driven algorithm, is much more efficient than the time-step driven algorithm, described in Section 2.2. Hence, unlike a time-step driven algorithm, it does not suffer from the decrease of the event probability with decreasing temperature. The N-fold way algorithm

was first introduced by Borzt, *et al.* in 1975 [27].

The problem with the N-fold way algorithm is that additional bookkeeping is required. This means that each individual time-step takes far more computational time than that of a time-driven algorithm. Another disadvantage of the N-fold way algorithm is that one loses the knowledge of how long a time a move would have taken to occur. To get an estimate on how long it would take for a move to occur, one can use Eq. (2.16) to be discussed.

The idea with the N-fold way is that one first realises that the number of possible local environments a spin can exist in is, for most systems, a rather small number, N. The name N-fold way originates from this fact. For example, for a spin having the value $s_{ij} = 1$ in an Ising square lattice, where $\mathbf{H} = 1$, there are 5 possible ways the nearest neighbours can arrange themselves in. The 5 different possibilities are illustrated in Fig. 2.3.

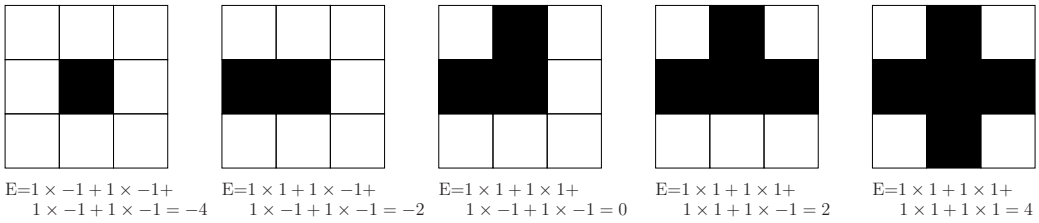

Figure 2.3: A picture depicting all the possible local energies a spin can have when the field is assumed to be constant and the spins interact only with nearest neighbours.

In the same way, we can do the same calculation for $s_{ij} = -1$. The number of possible energies we can have will not increase by flipping s_{ij}. An energy class is defined as a group in which spins with the same local energy reside. Then one spin can belong to one of 10 different energy classes. Accordingly, a list where spins are sorted in different energy classes must be created.

Once all the possible energy classes and the number of spins belonging to them is known, the probability of flipping a spin in class l is computed. The probability of a spin belonging to class l being flipped is

$$p_l = n_l e^{-\Delta E_l / k_B T}, \tag{2.13}$$

where n_l is the number of spins that belong to class l. This can be further simplified since the quantities

$$b_l = e^{-\Delta E_l / k_B T} \tag{2.14}$$

are constant throughout the whole simulation. The only thing that changes after a move is the number of particles, n_l, that belong to the energy class.

The next thing to do in the algorithm is to determine which spin to flip. This is done by generating a random number so that $0 < r_{num} < Q_N$. Q_N is the total probability of all the states, in other words,

$$Q_M = \sum_{l \leq M} p_l. \tag{2.15}$$

Now one only needs to find which energy class, l, the generated random number belongs to. This is done by finding $Q_{l-1} < r_{num} < Q_l$. Once this is known, a second random number is needed for selecting one of the n_l spins from the class. After this a third random number is needed for estimating how long it would have taken for this flip to occur in a time-step driven algorithm. The time estimate is obtained from

$$\Delta t = -\frac{\tau}{Q_N} \ln(r_{num_3}), \tag{2.16}$$

where τ is the time needed to execute a flip and Q_N is as defined in Eq. (2.15).

Once a spin has been flipped, one also needs to update the bookkeeping lists. The spin just flipped needs to be removed from its old energy class and added to the new one. In the same way all nearest-neighbour spins must also be updated, since they are also affected by the flip.

2.5 Kawasaki or spin-exchange dynamics

An update in the Ising model can be implemented by, for example, randomly picking a lattice site and then flipping the spin in it, i.e. changing s_i from -1 to 1. Another way of generating new states is to pick a site at random and then exchange the spins in it with some other spin on the lattice. This latter method is the so called Kawasaki, or spin-exchange, dynamics, first introduced by Kawasaki in 1972 [37].

Due to Kawasaki dynamics exchanging the values of two different spins, the total number of spins having the value 1, and correspondingly the value -1, is preserved throughout the whole simulation. This is very desirable when

the system studied consists entirely of particles, and no particles are added or removed throughout the entire simulation. One restriction needs to be added to this method if particles are being simulated and that is that only nearest-neighbour spins can exchange their values. This limitation is due to that no particle should be allowed to travel longer than one lattice site in one update. In other words, a particle is only allowed to move one step backward, forward, left, or right during one update.

When implementing the algorithm the following steps are needed:

1. Pick at random one site on the lattice.
2. Pick at random another site on the lattice.
3. Make a trial configuration where the two sites have exchanged their values.
4. Calculate the change in energy, ΔE, between the current configuration and the new trial configuration.
5. Depending on the change in energy, ΔE, accept or reject the new trial configuration.
6. Finally, update quantities, such as internal energy, if needed.

2.6 Hoshen-Kopelman cluster labeling algorithm

The Hoshen-Kopelman cluster labelling algorithm [38] is quite simple, yet not too obvious a method of finding clusters in, for example, an Ising simulation. The algorithm labels all the clusters with an increasing number for each newly found cluster during one scan over the lattice.

The algorithm starts from the lower left corner and then moves from left to right on that row. When it reaches the end of a row it continues on the row above starting from the left edge. When the algorithm starts on the first row it only checks for spins with $s_{i,1} = -1$, i.e. particles, that have a neighbour to the left. The first spin with $s_{i,1} = -1$ it finds on the first row is given the label 1. If this spin has a neighbour to the right, also with spin $s_{i+1,1} = -1$, then this spin is also given the label 1. If it later finds a spin without a neighbour, then this spin is assigned a different label. The new label is the one added to the most recently used label. When the algorithm has reached the end of the first row it continues to the row above. This time

it checks also the spins below and to the left. And in the same way as before, it assigns a label to this spin based on the labels the neighbouring spins have. A small problem will arise when the algorithm encounters a spin that has two neighbours. To solve this problem an array called *np* is introduced. If, for example, labels 1 through 5 have been used up to this point during the run of the algorithm then the array will be as follows:

np(1)	np(2)	np(3)	np(4)	np(5)
1	2	3	4	5

A proper label is a new concept that is introduced using this *np* array. If a spin has a proper label, it means that when one inserts the spin labels into the *np* array then the same number is returned from the array. The *np* array's main task is to link clusters together. For example, if two clusters having different labels meet at some point, then the *np* array is altered so that it returns the smaller of the two cluster labels, this way linking the two clusters together. In the following *np* array clusters 4 and 5 have merged.

np(1)	np(2)	np(3)	np(4)	np(5)
1	2	3	4	4

When the algorithm reaches a point where it finds a spin with two neighbours, it first checks if the two neighbours' labels are different. If they are the same, the spin is given the same label. If they differ, it determines the proper labels of the two spins using the *np* array. Then it assigns the lower proper label to the spin and sets *np* of the higher proper label to return the lower proper label. If a spin has only one neighbour, then just as on the first row, the spin is given the same label as the neighbour and no changes are made in the *np* array. When the algorithm has finished a pass through the array it does a second pass, where it replaces all improper labels with the corresponding proper ones. The end result is an array, with the same size as the one passed to this algorithm, where all the clusters have been labelled with different numbers.

2.7 The finite size scaling method

The finite size scaling method is a way of obtaining critical exponents by observing how systems of varying sizes behave [33, 39, 40, 41]. For example in the case of studying magnetic susceptibility an estimate of the critical

temperature, can also be obtained using the finite size scaling method. In our case where we will be studying the probability for the droplet to split during the simulation as a function of the field parameter, we will obtain an estimate of the critical field for when the probability to split will be 50%.

By first defining a new dimensionless function $\tilde{\chi}(x) = x^{-\gamma}\chi_0(x^{\nu})$, we get for the magnetic susceptibility

$$\tilde{\chi}\left(L^{1/\nu}t\right) = L^{-\gamma/\nu}\chi_L(t). \tag{2.17}$$

Here $\tilde{\chi}$ has been derived for the magnetic susceptibility in an Ising model. The exponent γ is and exponent that controls the singularity in the magnetic susceptibility and ν the correlation length for the Ising system.

The scaling function is the same for all systems; therefore we can expect that the estimates will fall on each other when we find the correct values of the critical parameters, γ and ν.

2.8 Random number generator

For generating the random numbers needed to run the simulations presented in this thesis we have used the random number generator known as the Mersenne Twister [42].

The Mersenne Twister is well suited for simulational purposes due to its extremely large period (it was designed to have a period of $2^{19937}-1$). It has a high order of dimensional equidistribution (the dimensionality is 623, which basically means that the correlation between successive random numbers is almost negligible), it is very fast and has passed numerous tests for statistical randomness, including the Diehard tests [42].

Chapter 3

Results

Results from simulations will be presented and discussed in this chapter. Many of the results rely on studying the centre-of-mass motion of droplets and looking at their modes of movement. The modes of movement are either calculated when the droplet is on a surface or travelling over a surface edge. A surface, sometimes also called a step, is an area where a single particle can move around without changing its energy. A step edge, or surface edge, will cause an energy change when a particle travels over it.

The physics of the motion of the droplet and the phenomena driving the droplet forward were studied using mainly one and two step configurations.

In the one step configurations the main goal was to determine the physics of the drop transportation over a potential step. The configurations of highest interest were ones where the droplet was placed right at the step (distance from step was zero particle lengths), symmetrically placed over the step, and where the droplet was moved away from the step with intervals of even distance. Later simulations containing multiple steps were studied.

In one set of simulations the step was even removed altogether. The purpose of removing the step was to learn how the diffusion of the droplet scaled as a function of the droplet size.

Later, runs were made using the Metropolis method, so that a comparison between that and the N-fold way could me made. The results these two methods yielded were then verified and indeed found similar. The biggest observed difference between the two methods was that the Monte Carlo method was much slower than the N-fold way at very low temperatures. This is as expected from the differences of the time- and event-driven algorithms, see Sections 2.3 and 2.4.

The droplet motion was typically analysed through observations of centre-of-mass motion and separate modes of motion in time.

The centre of mass motion was calculated using all the available particles in the simulation or by only using the particles that belong to the largest droplet. The particles belonging to the largest droplet were identified by using the Hoshen-Kopelman algorithm described in Section 2.6. However, in the simulations typically tracking the centre of mass motion of all particles was usually sufficient.

The other way used to characterise the droplet dynamics was observing "modes". Modes were defined to be the different ways in which a single particle can move. In total six different modes were identified. They were plotted as functions of time during the entire simulation. Modes can be classified according to how many particles surround the initial and final locations of the particle that was moved. Data for these modes were collected for any particle that moved over a step edge. Later the algorithm for identifying the different modes was modified so that modes present on a step could also be studied. Even though modes can now be collected and studied when particles move either on top of a step or over a step edge, it is still more interesting to study the case when particles move over a step edge, since it reveals the most dominant mechanisms in step crossing.

The width of the droplet was much smaller than that of the substrate in most of the early simulations. Later the substrate width was changed so that it was equal to the width of the droplet thus creating a periodically connected droplet. When the drop is as wide as the substrate, it will have to move down the steps using different mechanisms than if it was on a much wider substrate.

In simulations where the initial location of the droplet was very close to the edge of the first step, there were some very large differences in the modes according to whether the particles moved down the first or the second step. The time it takes for the droplet to find the first step is dependent on the distance from the first step edge.

To validate the implemented dynamics, we first simulated a droplet that moved on a substrate with no steps. As expected, the droplet moves by collective diffusion. The configurations obtained from simulations with no steps were later used as equilibrated initial configurations on stepped surfaces.

In the next subsection we describe the simulations which were performed to determine the droplet's centre-of-mass motion dependence on the number of steps, or potential drops on the surface, and also to see how the size of the

droplet influences the mechanisms that are driving it forward over the steps on the surface.

3.1 Single-particle processes driving the droplet forward over a step

The best way of studying how the droplet is moving over a step edge is by looking at how single particles are moving on the substrate. A similar method to what we are using here was described by T. D. Blake *et al.* in [43], where they looked at velocity distributions inside droplets using molecular dynamics simulations. Here we will take a closer look at what kind of particular moves occur when the droplet is translocating on the lattice. In total six different moves, or modes, can be identified by checking the number of neighbours present around a moving particle's initial and final location. The modes are denoted as:

1. **all ↔ all**
   Three neighbouring sites are filled around both the final and initial location of the particle.

2. **all ↔ one or more**
   All neighbouring sites are filled around the location where the particle is leaving from and one or two neighbouring particles are present around the final location.

3. **all ↔ none**
   The initial site is surrounded by three neighbours and the final site has no neighbours.

4. **one or more ↔ one or more**
   There is one or two neighbours around the site the particle leaves from and either one or two neighbours around its final location.

5. **one or more ↔ none**
   Either one or two particles are neighbouring the initial particle location and no particle is neighbouring its final location.

6. **none ↔ none**
   There are no neighbours neither around the particles initial location nor around its final location.

When quantifying the different types of moves, or modes, of the droplet motion, the particles moving in the direction of decreasing potential are counted cumulatively as a function of time. If a particle's move over a step edge increases the systems energy then the modes are decreased.

The way of studying the processes, as described above, were at first only meant to be used at the edge between two potential surfaces with different field parameters. The modes on top of constant potential surfaces depend on the number of particles on the surface in question. The more particles there are on a surface, the greater will the modes be when they are calculated from this surface. A normalisation is needed so that modes from different surfaces are comparable to each other. It was decided to study the flow of particles on surfaces, so basically the time derivatives of different modes were calculated.

The problem when looking at the modes by studying their velocities, or derivatives of the cumulants, is that they are dependent on the number of particles on the surface. In its initial position the droplet is completely on a surface and in time will slowly move away from this surface. As the droplet leaves the surface the modes will diminish toward zero. The potential difference between the constant potential surfaces will have a direct influence on the velocity of the mode being studied.

The solution to this problem was to normalise the modes. The modes were normalised so that their amplitude would be at most equal to one and also so that they would give a measure of how significant a specific mode is in comparison to the rest of the modes at a certain step and time, t.

The normalisation of the modes was done by summing up the absolute values of all modes and then dividing the individual modes with this sum as can be seen in Eq. (3.1). The result is that the modes will now have a value between minus one and one. This made it possible to compare how significant a role a single mode has compared to other modes.

$$M_{norm,i}(t) = \frac{M_i(t)}{\sum_{i=1}^{6} |M_i(t)|}. \tag{3.1}$$

Data was collected from two systems, one with five and one with 21 steps, the data for the modes on the steps was then normalised and analysed. The observed difference between the modes on different steps is that on the first steps the modes for the **all** $\leftrightarrow$ **all** and **none** $\leftrightarrow$ **none** are very similar. But as the step number grows the difference between these two modes will grow. A possible explanation for this is that **none** $\leftrightarrow$ **none** moves will always be present on every step while **all** $\leftrightarrow$ **all** moves will only occur when the droplet

is crossing the terrace edge in question. It is only natural that the last step shows a higher amount of **all** ↔ **all** moves since in its starting configuration all steps are located underneath the drop. As the droplet is moving over the steps it spends the most time on the last step and the least time on the first step. Therefore, a difference is seen in the modes directly reflecting the time spent on a specific step.

In Fig. 3.1 the modes for the fourth step in a simulation with a total of 22 different constant-potential surfaces, or 21 potential drops are shown. The mode graphs for the first three steps are not shown since they show very random mode behaviour. The mode graphs for the first step are naturally neglected since the droplet never actually is on the first step. The configuration is chosen so that when the droplet is in its initial configuration all steps, except the first and the last, are under it. That means the first step edge is where the droplet starts and the last step edge is where it ends.

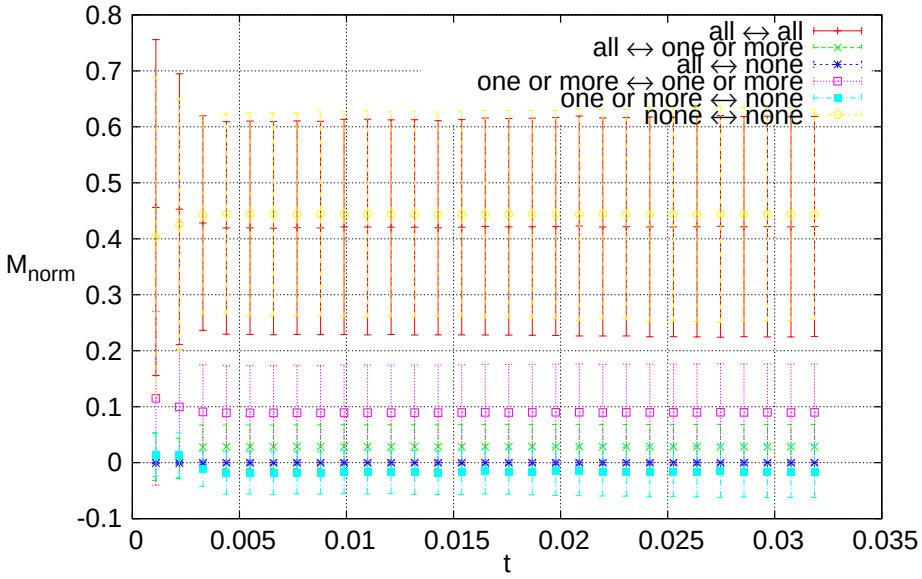

Figure 3.1: Normalised mode graphs, M_{norm}, as a function of time, t, for the fourth step in a simulation with 22 different potential surfaces.

In Fig. 3.1 the graphs for the **all** ↔ **all** and the **none** ↔ **none** normalised modes are nearly identical, but when comparing these modes to the same modes on the last step in the same simulation the situation is slightly different, as can be seen in Fig. 3.2.

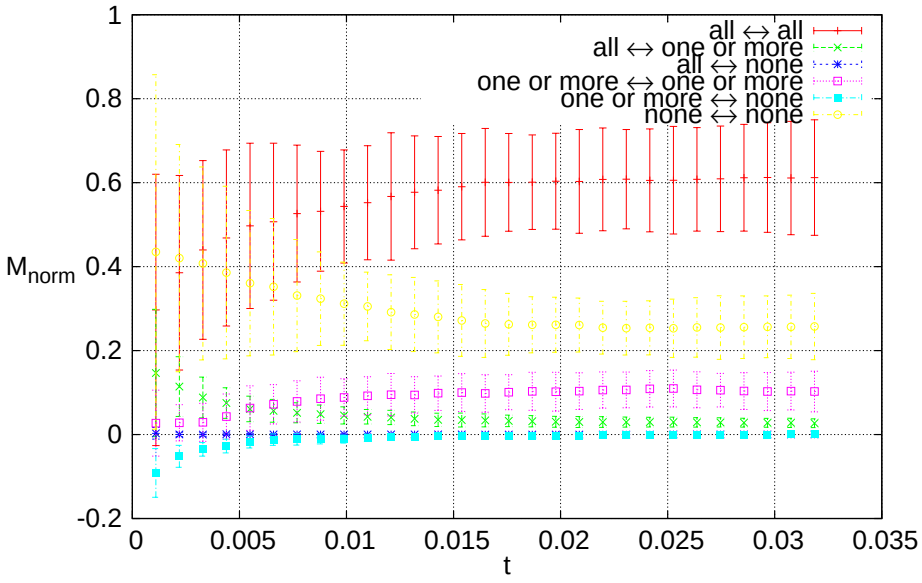

Figure 3.2: Normalised mode graphs, M_{norm}, as a function of time, t, for the last step in a simulation with 22 different potential surfaces.

In Fig. 3.2 there is a clear difference between the two modes. The **all** ↔ **all** mode is clearly more significant than the **none** ↔ **none** mode. The droplet is still being driven forward by the field when it is on the fourth step. As long as it is being driven forward it has a narrower shape, which enables individual particles to freely move up and down over the steps. The droplet spreads as it reaches the last step and no potential is pulling it forward anymore. As its width grows it hinders the motion of randomly diffusing particles. Hence, the **none** ↔ **none** mode will grow smaller. There is no step edge that can rip particles away from the droplet when the drop has reached the final step. There are step edges that can pull particles away from the droplet as it is moving over the step edges in the middle of the lattice. Hence, these particles contribute to the magnitude of the **none** ↔ **none** mode.

Next we will look at how the droplet's size affects the modes, counted at the step edge, as a function of the field parameter. We normalise the modes, according to Eq. (3.1), to get a view of how strong a specific mode is in comparison to the rest of the modes.

We show in Fig. 3.3 the modes as functions of time for two systems. The first system has a droplet of size $L_x \times L_y = 80 \times 80$ and the second of size $L_x \times L_y = 160 \times 160$. The mode values presented in these figures were

read from the simulations at the moment when the droplet divided into two droplets.

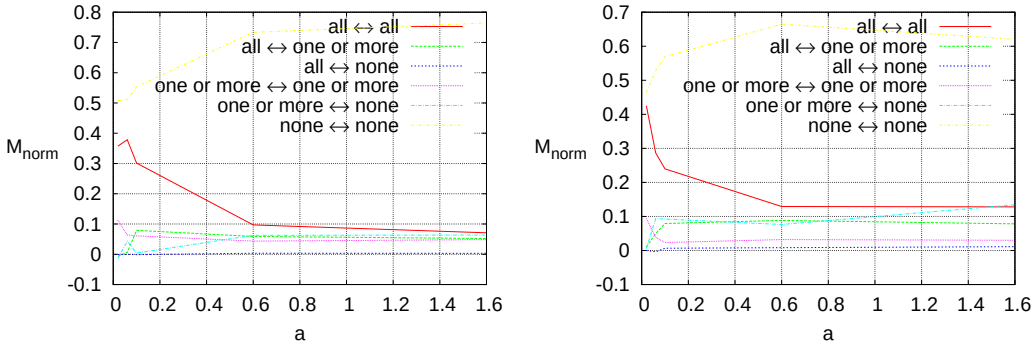

Figure 3.3: Normalised modes, M_{norm}, as a function of the field, a, for a system containing a droplet of size **(a)** $L_x \times L_y = 80 \times 80$. **(b)** $L_x \times L_y = 160 \times 160$.

We see from these figures that the driving processes are the same, even if the droplet size is increased. The **all** $\leftrightarrow$ **all** mode tends to be more active at lower fields. Its significance drops rapidly as the field is raised. The **none** $\leftrightarrow$ **none** mode is in all cases the most active mode. The **none** $\leftrightarrow$ **none** mode, accounts for single particles moving over the step edge, and is called accordingly the diffusion mode. In these simulations we are more interested in studying how particles connected to the translocating droplet move.

Worth noting here is what we found when looking at how the modes differ for different sized droplets. We found that at high fields there is another mode that plays a significant role in transferring particles across the step edge, namely the **one or more** $\leftrightarrow$ **none** mode. In Fig. 3.4 the normalised modes are shown for a system with a droplet of size $L_x \times L_y = 120 \times 120$ and field a=1.6. The droplet used was initially located at zero distance from the step edge. The droplet splits into two separate droplets at around $t_{split} = 4.3 \times 10^{-4}$, after this the **one or more** $\leftrightarrow$ **none** mode increases quicker than any other mode. For this mode to be active there needs to be one or more neighbouring sites filled around the particle when it is above the step edge. Below the step edge there may not be any filled sites, this is a prerequisite for a positive **one or more** $\leftrightarrow$ **none** move. This is possible, for example if the particle existed paired with another particle and as it moved over the step edge the pair would split. Another option is for the particle to exist in a larger cluster of particles above the step edge and as it moves over the edge it gets separated from the cluster. However, no sign of such

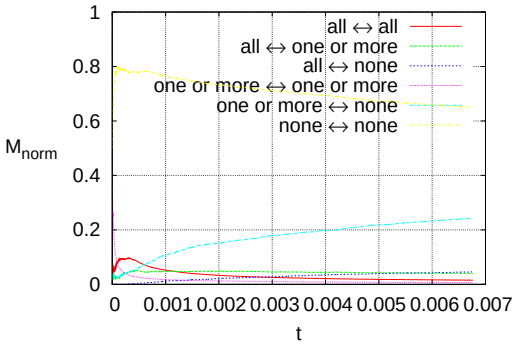

Figure 3.4: Normalised modes, M_{norm}, as a function of time, t, from a system with a droplet of size $L_x \times L_y = 120 \times 120$. Field a=1.6.

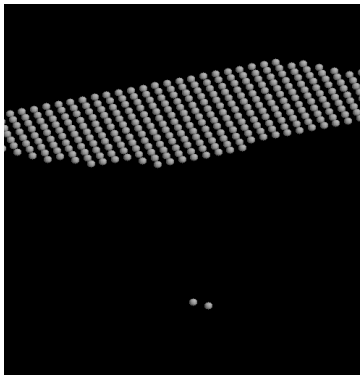

Figure 3.5: A pair of particles as observed in a simulation with one step edge.

clusters were seen in snapshots. Fig. 3.5 shows a magnification of a snapshot where a particle pair was found. Particle pairs, like the one in Fig. 3.5 are very short-lived. The higher the temperature, the lower is the probability for them to stick together.

At the beginning of the simulation we see, in Fig. 3.4, a slight increase in the **all** $\leftrightarrow$ **all** mode and the modes responsible for particles detaching from the droplet. The particles that move over the step edge are unable to move back since the field is very high, this creating a gap between the droplet and the step edge. Now the only mechanism able to transfer the particles over the step edge is the **none** $\leftrightarrow$ **none** mode. Hence, it is more active than the other modes after the start of the simulation.

3.2 Centre-of-mass velocity dependence on periodic droplet's side length

In this section we study a periodic droplet located over the step edge. By a periodic droplet we mean one whose width is the same as the width of the lattice on which it is simulated on, i.e. $L_x = m$, or $\Delta x = 0$, see Figs. 3.6 and 3.22. Δx is the distance from the droplet's edge to the edge of the lattice when the droplet is in its initial location. The droplet was made periodic to eliminate some processes for the system to serve as a reference model for droplet translocation.

In the case where the simulated system contained only one step, the droplet

initially located symmetrically over the step edge. If the simulation contained several steps the droplet was placed between the step edges of the first and the last step. These two configurations are shown in Figs. 3.6 (a) and (b). The reason for having the droplet start from a position, where the steps lie under it, was to eliminate the variation due to distance from the step edge. If the droplet is initially placed at a finite distance from the step edge then the time it takes for the droplet to reach the step will differ from one simulation to another.

The question addressed with these simulations is how the droplet width and length affects the centre-of-mass velocity and modes.

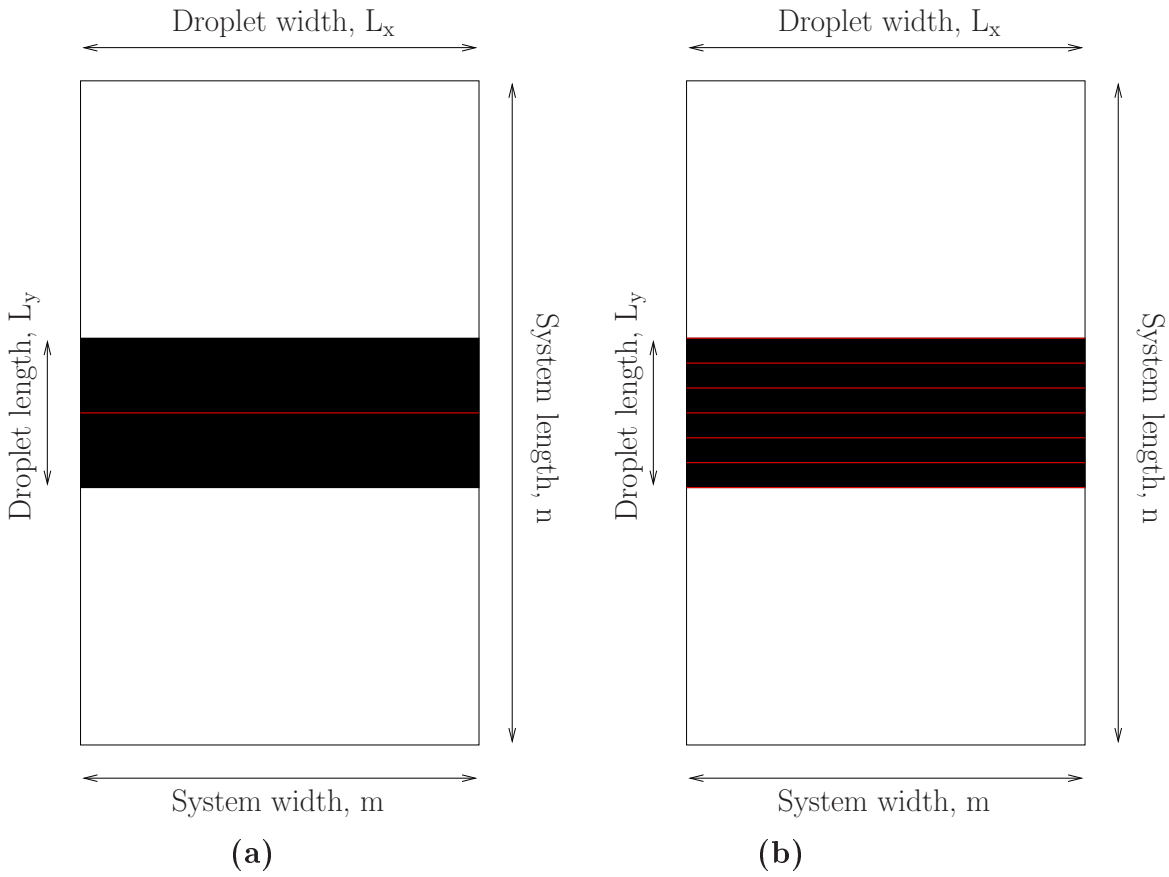

Figure 3.6: The setups used in these simulations were all of the type shown in this picture. The system length n was fixed at $n = 300$, while m, the system width, was changed, so that Δx would stay the same for all simulations in one set. Later, in Chapter 3.5, different values of Δx were used. A red line symbolises the location of a potential step edge.

By making the droplet periodic the potential subtleties due the initial configuration being not in equilibrium are eliminated. The periodic droplet serves as a simple reference for gaining understanding on the non-periodic droplet, to be described later.

When keeping the length of the droplet fixed and varying only the width, the intuitive guess is that all droplets should move with the same velocity over the step. This was confirmed by running several simulations for droplets of varying widths. In Fig. 3.7 centre of mass positions are plotted as functions of time for these systems.

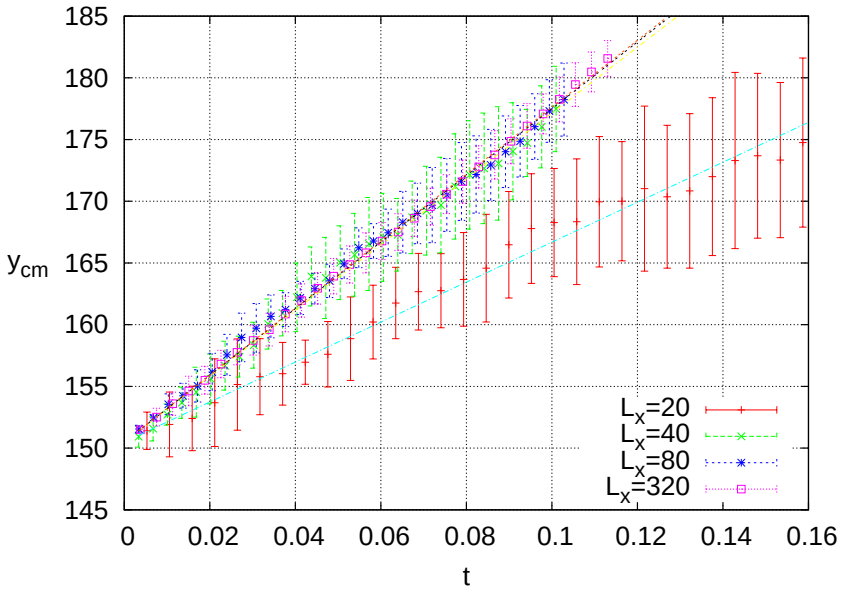

Figure 3.7: Centre-of-mass positions, y_{cm}, as functions of time, t, for simulations with periodic droplets of the size ($L_x \times L_y$) 20×80, 40×80, 80×80, and 320×80. The data presented in these plots have been averaged over 5 iterations.

The only droplet that appears to be moving at a velocity different from the rest in Fig. 3.7 is the smallest droplet, whose width $L_x = 20$. The centre-of-mass plot of this droplet is not as smooth as for the other droplets, instead in the individual runs there are regions where the velocity is very close to zero. The fluctuations in the velocity at these regions are explainable by freely moving particles that randomly move around, behind and in front of the droplet. From snapshots of the droplet in a zero velocity stage it was found that the front and back edges of the droplet are almost perfectly smooth. This would indicate that the droplet reaches a configuration where perturbing it

will require a lot of energy and hence will have a very low probability of occurring, in other words the droplet is in a local energy minimum. The droplet will start moving once enough particles have broken away from it and it has again reached an unstable configuration that can move over the potential edge more easily. At this point it was checked, whether the precision of the floating point numbers played any role in this phenomenon where plateaus appear in the plots for the smallest systems. It was found that when increasing the precision the step-like looking behaviour would also decrease.

Next, the length was varied while keeping the width constant. Using the results from these simulations we were able to verify that our model worked properly.

There is a very simple relation between the centre-of-mass velocity and the the length of the droplet that our model is required to produce in order to work properly. When we simulate a periodic droplet we have a case where mass is being transferred over a step edge with a constant velocity. Varying the length of the step edge will change the amount of mass being transferred over it as a function of time.

The centre-of-mass velocity is expected to obey

$$v_{cm}^{y} \sim \frac{1}{L_y}. \tag{3.2}$$

This is obtained as follows. The centre-of-mass is

$$\begin{aligned} v_{cm}^{y} &= \frac{\mathrm{d}y_{cm}}{\mathrm{d}t} = \frac{\mathrm{d}}{\mathrm{d}t}\left[\frac{\sum_{i=1}^{N} m_i y_i}{\sum_{i=1}^{N} m_i}\right] = \\ &= \frac{\mathrm{d}}{\mathrm{d}t}\left[\frac{mL_x \sum_{i=1}^{L_y} y_i}{mL_x L_y}\right] = \frac{1}{L_y}\frac{\mathrm{d}}{\mathrm{d}t}\left[\sum_{i=1}^{L_y} y_i\right], \end{aligned} \tag{3.3}$$

so for Eq. (3.2) to hold we must have

$$\frac{\mathrm{d}}{\mathrm{d}t}\left[\sum_{i=1}^{L_y} y_i\right] = C \quad \Rightarrow \quad \sum_{i=1}^{L_y} y_i \sim Ct, \tag{3.4}$$

where C is a constant.

Eq. (3.4) states that the sum of all particles y-coordinates will change linearly with time. This is exactly what we have, each update in y-direction will change the centre of mass coordinate linearly.

The velocities we obtained for 80,100, 120, 140 and 160 particles long droplets are shown in Table 3.1.

Table 3.1: Velocities for periodic droplets of the size $L_x \times L_y$ =80 $\times$ 80, 80 $\times$ 100, 80 $\times$ 120, 80 $\times$ 140 and 80 $\times$ 160. The velocities presented in this table have been averaged over five iterations. The field parameter was $a = 0.1$.

velocity	$L_y = 80$	$L_y = 100$	$L_y = 120$	$L_y = 140$	$L_y = 160$
mean	2562.6	2108.1	1786.0	1485.0	1362.8
std	371.21	284.41	154.68	49.22	150.71

In Fig. 3.8 Eq. (3.2) is fitted to the data in Table 3.1.

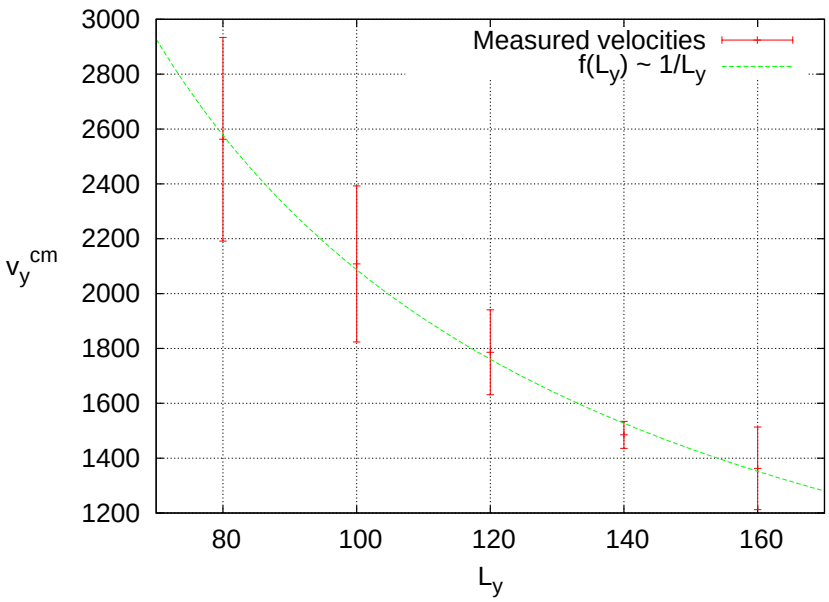

Figure 3.8: Centre-of-mass velocities, v_y^{cm}, plotted as functions of the droplet length, L_y. The velocity data plotted in graphs is shown in Table 3.1. The function $f(x)$ has the form $f(x) \sim 1/x$. Field $a = 0.1$.

The centre-of-mass velocities of different-sized droplets conform with the expected behaviour quite precisely. This serves as one validation for the implementation. We checked these results also using the same system at a lower field, $a = 0.01$ instead of $a = 0.1$, which was used in Table 3.1 and Fig. 3.8.

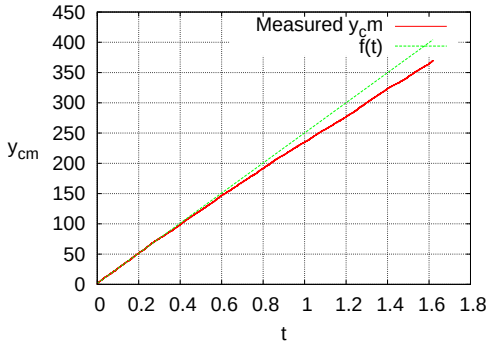

Figure 3.9: Centre-of-mass y-coordinate, y_{cm}, as a function of time, t, for a periodic droplet with size $L_x \times L_y = 80 \times 900$. We have fitted a line to the points where $t \in [0, 0.2]$ to better illustrate the non-linear transfer of particles across the step edge.

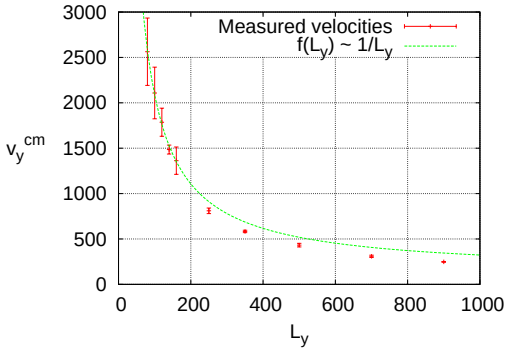

Figure 3.10: Data from considerably longer systems added to the graph in Fig. 3.8. A decrease in velocity, compared to what is expected from the model, is observed at long droplet lengths.

While studying the velocities of periodic droplets we came across an interesting phenomenon that causes the centre-of-mass velocities to diverge from the assumed $v_y^{cm} \sim 1/L_y$ dependency. We already know that the only mode that causes a periodic droplet to move over a step edge is the **all** $\leftrightarrow$ **all** mode, i.e. holes inside the droplet moving in the direction opposite to the droplet movement. If we create a very long droplet, we will have the case where each hole can be treated as a random walker that needs to find the step edge. The distance $|d|$ a random walker travels in N time-steps obeys $|d| \sim \sqrt{N}$. From this we can understand that the longer the distance is between the edge of the droplet and the step edge the longer it will take before a hole has travelled through the droplet to the boundary, which is directly reflected in the droplet translocation.

If the droplet is short we have a linear dependence between the travelled distance and the required time. In Fig. 3.9 we show the centre-of-mass y-coordinate for a $L_y = 900$ long droplet and in Fig. 3.10 we show the same data as in Fig. 3.8 together with centre-of-mass velocities taken from considerably longer droplets. The function $f(x)$ is the same in both figures. In the latter graph we see how long droplets deviate from the predicted model and translocate slower than what is expected. Initially, the droplet was placed over the step edge.

Later, systems with free droplets will be simulated. Since we know from the

simulations that at short times periodic droplets move like a solid flow we can make the conclusion that any differences in the centre-of-mass velocity between these two types of systems will be due to particles moving along edges of the droplet.

3.3 Centre-of-mass velocity saturation for periodic droplets at increasing fields

The droplet's size is 80×80 and it is initially located symmetrically over the step edge, i.e. the same number of particles are located above and below the edge. In these simulations one more potential gradient, or step edge, is added. As the simulation is initiated, the droplet starts moving over the edge. Depending on the field parameter the droplet moves with different velocities as it travels over the step edge. Fig. 3.11 (a) shows centre-of-mass velocities plotted as a function of the field.

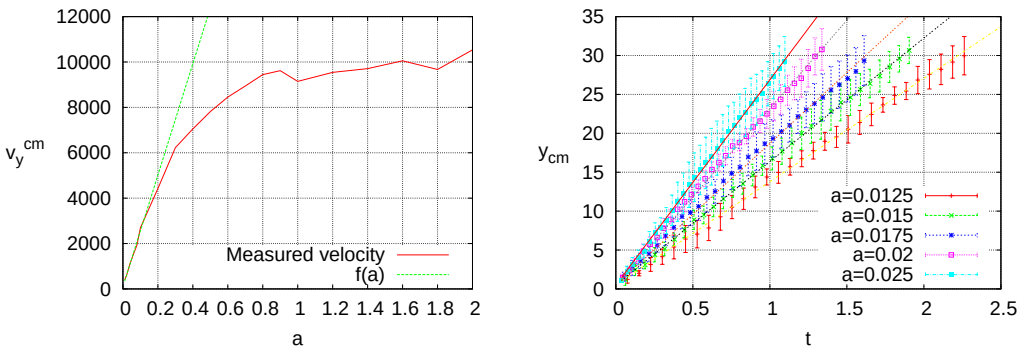

(a) **(b)**

Figure 3.11: **(a)** Centre-of-mass velocities in the y-direction, v_y^{cm}, as functions of the field parameter, a, for simulations with periodic droplets of size 80×80. The velocity is seen to saturate as the field is increased. A line was fitted to the data for $a \in [0.01, 0.1]$ to show the linear dependence between the velocity and the field parameter, a, at low values. **(b)** The same data plotted as centre-of-mass position, y_{cm}, versus time, t, graphs for different fields, a.

As can be seen from Fig. 3.11 (a), when the field is raised the centre-of-mass velocity approaches an upper limit. In Fig. 3.11 (b) we show centre-of-mass positions, as functions of time, for the 80×80 system at different field values, a. Later in Chapter 3.5, when we talk about how non-periodic and periodic droplets' centre-of-mass velocity depend on the field, we will come

back to these results. Later we will introduce a method of increasing the droplet velocity beyond this saturation value. To accomplish this, several steps have to be added. Systems with several steps will be studied further in Chapter 3.8.

At very low fields we noticed that the relation between particle velocity in y-direction and the applied field is linear. In Fig. 3.11 (a) a line is fitted to the data to illustrate the linearity at low field values.

The only perceivable reason for the velocity saturation of a periodic droplet at higher fields is the hole movements inside the droplet. At very low fields a hole, or a particle, has a finite probability of moving in "the wrong" direction. (The "wrong" direction stands for a hole moving down, or correspondingly, a particle moving up a step.) This probability is of the order of a hole moving randomly inside the droplet. As the field is raised the probability for the holes to move in the wrong direction is decreased. The absolute upper limit for saturation to occur in a simulation is when the probability for a hole to move in the wrong direction becomes so small that it is no longer representable using double precision floating point numbers.

To investigate if holes play a significant role in the droplet's centre-of-mass velocity dependence on the field parameter, we simulated two systems and recorded the number of particles moving in the two available directions over a step. The number of particles having moved over the step edge (in the positive direction) is shown in Table 3.2 as a function of time. A similar table can be made for the particles going in the opposite direction though it was chosen only to show one of the two cases due to their great similarity. In the end of the simulations the net flow differs only on the order of the number of particles in the droplet, in this case 1600.

Table 3.2: The number of particles that move inside the droplet up the step edge (in the "wrong" direction) has been recorded for one system at two different field values. $\Delta n/\Delta t$ is is the frequency at which holes move over the edge.

	$a = 0.0125$	$a = 0.4$
$\Delta n/\Delta t$	1.2×10^6	1.4×10^5

There are dramatically more particles flowing up the step edge in the case where $a = 0.0125$ since the probability for a particle to go back up the step edge is close to the probability of a particle randomly moving around. As the field parameter is raised, the number of particles moving over this edge

is decreased, dramatically as can be seen in Table 3.2. This is due to the significant decrease of the probability for a particle to move up the step edge. The simulation at the higher field ran a much shorter time due to this phenomenon, hence the much shorter line in this graph.

The time it will take for a particle to move up over a step edge can be shown to be linearly dependent on the field parameter.

We find from Eq. (2.16) in Section 2.4 how to calculate the time for individual updates in the simulation.

If we want to calculate how long a specific update, causing the system to change energy ΔE_k, will take, we have to use

$$\Delta t = -\frac{\tau}{Q_l} \ln P\,(t),$$

where Q_l is as described in Eq. (2.15). The probability for the system to go through a change increasing its energy with ΔE_l is calculated from Eq. (2.12). When a particle moves up a step it will increase the systems energy, ΔE_l.

By inserting Eq. (2.12), for the case of $\Delta E_l > 0$, into Eq. (3.3) we get

$$\Delta t = \frac{\tau}{Q_l} \frac{\Delta E_l}{k_B T}.$$

We know the Hamiltonian for the system from Eq. (2.1). The energy change is linearly dependent on the field parameter, $\Delta E \sim a$, if the only change to the system is a particle moving up a step. In other words, particles will easily move over the step edge in the direction which decreases the system's total energy, but the higher the field, the longer will it take for them to move in the opposite direction. Movement in both directions take place until the probability is small enough to no longer cause a significant flow of particles, resulting in saturation of the centre-of-mass velocity. Since the dynamics inside the droplet is crucial for periodic droplets, the field dependence of this dynamics determines the droplet motion.

Finally, we show mode graphs of periodic systems for later reference.

Fig. 3.12 shows modes for a typical periodic droplet. The data for the modes in this figure are collected by counting how many particles move over a step edge and identifying the modes they belong to. For periodic droplets there obviously is only one mode that is significantly larger than the rest, namely the **all** $\leftrightarrow$ **all** mode. The predominance of the **all** $\leftrightarrow$ **all** mode in the periodic droplet is the reason for using it to investigate dynamics taking place inside the droplet, see discussion above.

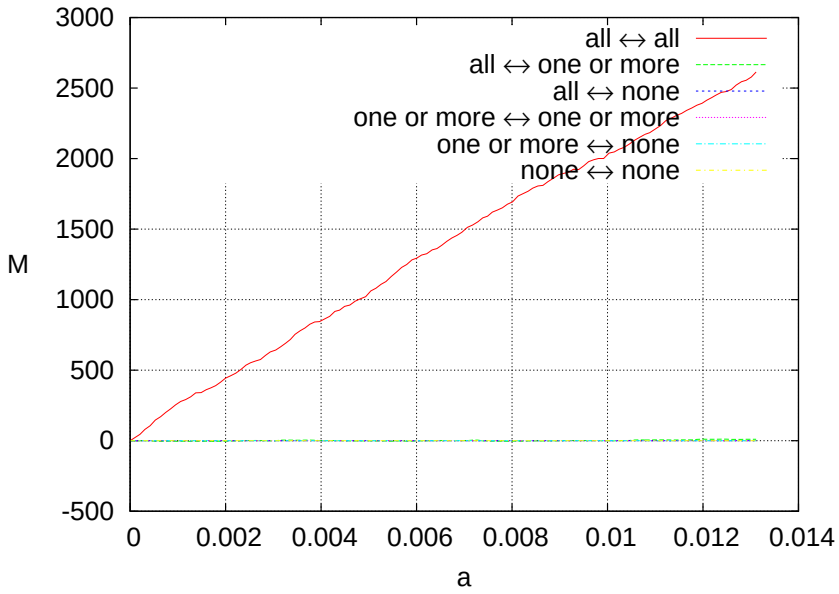

Figure 3.12: Modes, M, are plotted are a function of time, t. The data for this graph was collected by counting how many particles belonging to each mode moves over a step edge. The modes shown here were taken from a system with a 80×80 large droplet at field $a = 0.1$.

However, the **all** $\leftrightarrow$ **all** mode is not the only mode active in a periodic droplet. There are also **one or more** $\leftrightarrow$ **one or more** and **one or more** $\leftrightarrow$ **none** moves taking place. Both of these modes take place at the back and front edge of the droplet. For a hole to be created a particle has to break off from the edge of the droplet.

As the field is lowered in a periodic simulation we will obtain mode graphs very similar to the ones shown in Fig. 3.12.

3.4 Cross-over from periodic to free droplet motion when increasing substrate width

In order to validate our model for simulating droplet dynamics and to investigate hole dynamics inside the droplet we have been looking at droplets in periodic systems up to this chapter. The true interest, of course, lies in the characterisation of the dynamics of an unconstrained, or non-periodic droplet, which we shall call free. In Fig. 3.13 we show an image of a typical

setup for a non-periodic system.

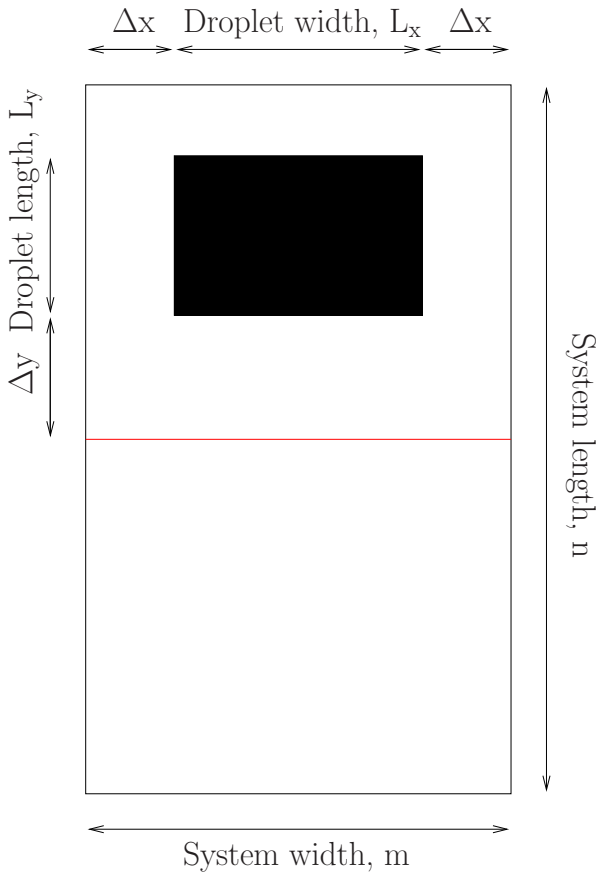

Figure 3.13: A setup for a non-periodic system. The distance from the edge of the lattice to the edge of the droplet in x-direction is denoted by Δx, and from the lower edge to the step edge be Δy.

By studying a droplet of constant size in various fields we determined how the centre-of-mass velocity for the droplet depends on the field. However, first we look briefly at how the distance from the droplet boundary, to the edge of the lattice, Δx, affects the centre-of-mass velocity. The free droplets in these simulation are all nonequilibrated. The simulated droplet motion starting from an equilibrated and a nonequilibrated configuration, were found identical, as will be described in Chapter 3.8.

It was mentioned in the previous chapter that periodic droplets of constant length will move over a step with the same velocity regardless of the width of the system. The results from simulations of periodic droplets no longer

hold when the width of a nonperiodic system is varied. It was found that the centre-of-mass velocity is dependent on the droplet width, L_x, in a non periodic system. These results were obtained from a simulation with one step when using a nonperiodic droplet.

Next, two new cases of this phenomenon are going to be discussed and analysed. In the first case the distance between the droplet boundary and the substrate edge was gradually increased from $\Delta x = 5$ to $\Delta x = 200$. It was found at $\Delta x > 100$ the droplet motion is not affected by the substrate edge.

In Fig. 3.14 the centre-of-mass velocities, v_y^{cm}, are plotted as functions of droplet width, L_x. In this figure droplets placed at varying distances from the edge of the lattice are compared. All the droplets were initially located over the step edge.

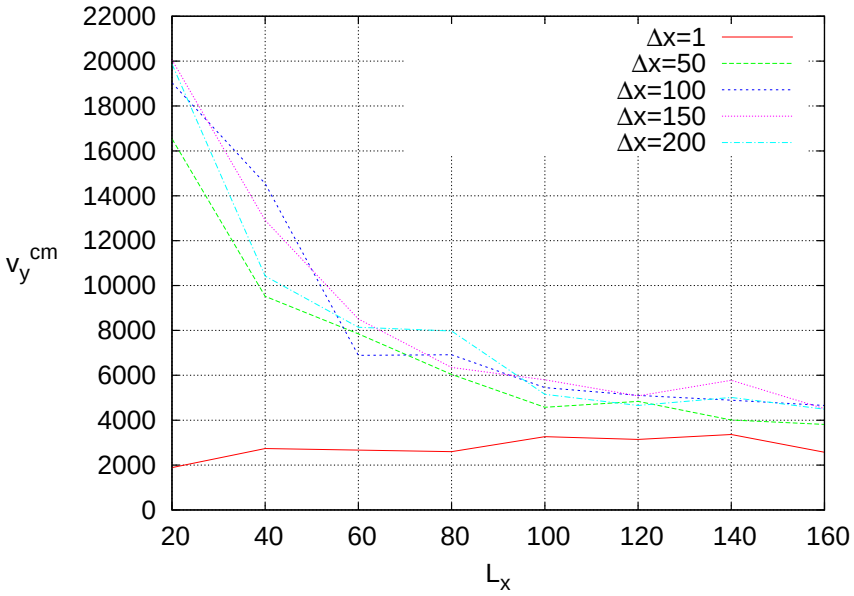

Figure 3.14: Droplet velocity in y-direction, v_y^{cm}, is plotted as a function of droplet width, L_x. Droplet length is fixed at $L_y = 80$. Various substrate widths, Δx are compared. For the narrowest substrate, $\Delta x = 1$, we in practise have a periodic system.

The droplet for which $\Delta x = 1$ resides on a substrate that is only two particle lengths wider than the droplet itself. So, in practise it is a periodic droplet. Comparing the plot where $\Delta x = 100$ to the one where $\Delta x = 200$ show no change in the droplet velocity within the statistical error. This gives an estimate for the distance individual particles or particle pairs may travel in

the direction aligned with the step edge before being driven onto the lower step. For $\Delta x = 1$, one droplet, namely the most narrow one, for which $L_x = 20$, has a slightly lower velocity than the other droplets. This was found to be due to an artifact that occurs when simulating very narrow droplets in periodic systems. This unphysical behaviour was found to decrease when the floating point number precision was raised. The precision used throughout all the simulations was double precision but long double was used for testing the theory that the difference in velocities comes from a lack of numerical precision. Due to the dramatic increase in the needed simulation time it was decided to continue using double precision floating point numbers. However, to avoid artifacts like this, it was decided not to use droplets of this length scale, 20, or smaller.

Another observation can also be made from Fig. 3.14. When Δx is large, a smaller droplet moves faster over the steps.

From these simulations we know that having a gap of at least $\Delta x = 100$ is enough. In other words, this is the distance at which there is a significant amount of individual particles or very small clusters, typically of the size two, crossing the step edge.

3.5 Variation of the centre-of-mass velocity with varying low field

Having determined the minimum distance between the droplet and the substrate edge to have droplet motion free from boundary effects, we turn our attention to how the field affects the centre-of-mass velocity of periodic and free droplets.

If one simplisticly assumes that the collective motion of an undeformed droplet is determined by transfer rates deduced from transfer rates of individual particles, one could hope for the centre-of-mass velocity to have a form $v_i^{cm} \sim e^{ka_i}$, where a_i is the field parameter and k is a constant. The above equation is obtained by assuming that the velocity when a particle moves over a step, is proportional to the transition probabilities of the individual particles inside droplet, $W \sim e^{-\Delta E/k_B T}$. If there is a change in the field parameter then $\frac{W}{W_0} \sim \frac{e^{-\Delta E/k_B T}}{e^{-\Delta E_0/k_B T}} \approx e^{k\Delta a} = A$. Here A is assumed to be proportional to the droplet velocity and k is a system independent constant. Accordingly, between two different simulations, indexed i and $i+1$, it should hold that $v_{i+1}^{cm}/v_i^{cm} = e^{k(a_{i+1}-a_i)}$.

This relation was verified by running simulations on one system with field parameters $a_i = (i+1)\cdot 0.0025$, see Table 3.3. The data in Table 3.3 was taken from simulations of a free droplet consisting of 80×80 particles. The velocity data for the droplets at varying fields have been measured in the beginning of the simulations and averaged over five iterations. As the field parameters a_{i+1} and a_i are raised the corresponding k values k_i tend to decrease, so obviously either there is a physical reason for this k or the exponential form does not describe the translocation dynamics of the droplet particles.

Table 3.3: k values for the dependence $v_{i+1}^{cm}/v_i^{cm} = e^{k(a_{i+1}-a_i)}$.

	k_1	k_2	k_3	k_4
free droplet	71.32	69.82	37.89	35.97
periodic droplet	70.97	54.79	88.20	30.21

In Fig. 3.15 the centre-of-mass velocities v_y^{cm} for both free and periodic droplets are plotted as functions of the field a. v_y^{cm} is seen to depend roughly linearly on a. Since ka_i is of the order of 1 even for the weakest fields, the Taylor expansion $v_i^{cm} = e^{ka_i} \approx 1 + ka_i + \left[\frac{1}{2}(ka_i)^2 + \ldots\right]$ cannot explain this dependence.

Comparing the free droplet motion to that of the periodic droplet, one sees that the linear dependence coming from the flow of the droplet as a continuous mass, evident from the centre-of-mass movement of periodic droplets, also dominates the ballistic motion of the free droplet, even though there is a substantial contribution from driven diffusion of individual particles outside of the free droplet. The field dependence in the periodic droplet has to come entirely from the hole movement, see Section 3.3. Due to the similarity of the field dependence of the periodic and free droplets the hole dynamics inside the droplet has to play a significant role also in the case of free droplets. This observation will be further confirmed when investigating droplet motion over multiple steps, see Section 3.8. When raising the field we decrease the probability for holes to move in the direction where they increase their energy. We observe saturation of the droplet's centre-of-mass velocity when holes are no longer able to move in this "wrong" direction to accommodate more particles on the lower step. The field dependence of the droplet velocity at higher fields will be dealt with in the next section investigating transition between diffusive and ballistic motion.

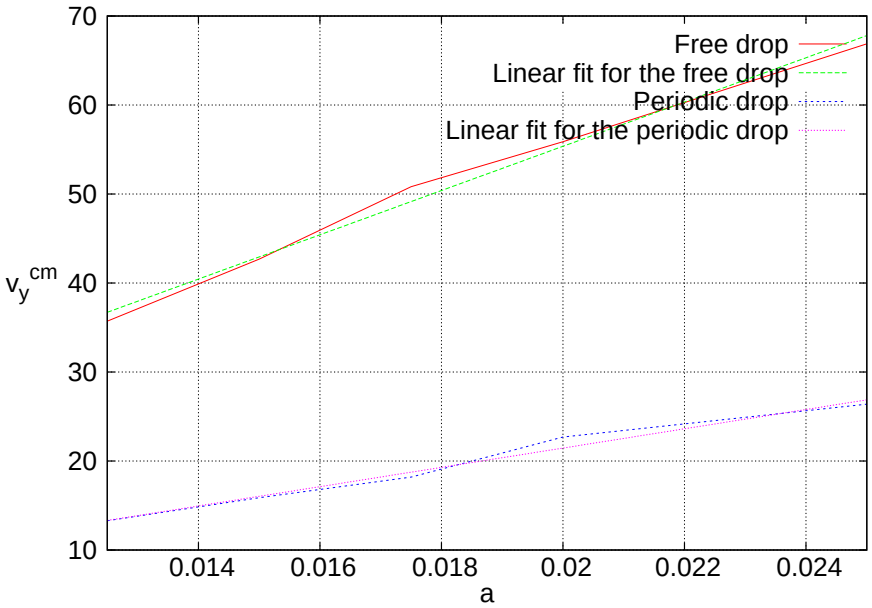

Figure 3.15: Centre-of-mass velocities, v_y^{cm}, plotted as functions of field parameter, a. The slope, k, for the fitted lines corresponding to the free droplet is $k \approx 2480$. The slope for the periodic droplet is $k \approx 1080$.

3.6 Regimes of ballistic and diffusive motion

This section discusses how various droplet sizes, magnitude of field, and number of steps affect the outcome of the simulation and also why these results are observed. Some concerns about the used setup in the initial simulations will be raised and a motivation for why the systems studied later in this section differs from these systems will be given.

The results described here were generated by simulations with one step and a 40×40 or 80×80 droplet. The starting location for the droplet is on the constant potential surface above the first step. The initial distance to the step edge was fixed to one particle length. The distance from the droplet to the substrate sides in x-direction, Δx, was kept constant at 110 lattice intervals, or particle lengths. A sample setup is shown in Fig. 3.13. Δy has usually been on the scale of a few lattice sites, i.e. $\Delta y = 1$ or $\Delta y = 2$.

As the field is raised it was observed that the velocity, with which the droplet moves, increases until the field gets high enough for the droplet to start breaking up into two (or more) droplets. The most common droplet behaviour for fields that are very high is that two droplets are formed from the original. A

Table 3.4: Centre-of-mass velocities for 40×40 and 80×80 droplets. The velocities are shown for various field parameters.

Droplet size	$a = 0.02$	$a = 0.04$	$a = 0.2$	$a = 0.8$
40x40	2657.8	5369.3	27903.3	52418.2
80x80	1247.9	2428.8	11442.2	16416.8

new droplet appears somewhere on the lower step while another will be in the original droplet position. In a simulation where the droplet flows smoothly over the step edge particles are constantly moving up and down over the step edge but the net flow of particles is in the direction in which the individual particles experience a smaller energy. At a critical field value it gets energetically more favourable for the droplet to divide into several droplets and move through driven diffusion of single particles to the lower step.

In Fig. 3.16 centre-of-mass velocities, in y-direction, are shown as functions of the field parameter. When the field parameter is raised the centre of mass velocity for the droplet will saturate. When the centre of mass velocity is beginning to saturate the droplet starts to move over the step, not as a single droplet but through individual particles that have broken free from it on the step with higher potential. These particles are then collected on the lower step, where they start forming a new droplet. The absolute limit for when saturation occurs is when the probability of a particle that is moving up a step, in other words increasing its energy, gets smaller than what is representable using floating point numbers.

When the size of the droplet is increased, the centre of mass velocity will normally decrease, since more particles have to be moved over the step edge. In Table 3.4 are centre-of-mass velocities shown for both the 40×40 and the 80×80 system in Fig. 3.16.

The centre-of-mass velocity increases linearly with the field parameter at low values, $v_y^{cm}(a) \sim a$. In this case only fields $a = 0.02$, $a = 0.04$ and $a = 0.2$ are well described by the linear dependence. The highest field, $a = 0.8$ is close to the saturation limit, i.e. droplet breakage, and does not fall into the linear regime.

Next, we will look at how the temperature and field affects the motion of the free droplet. When the temperature is increased, the droplet will move faster over the step edge, since particles now have a greater probability of breaking away from the droplet and moving over the step edge. At very low temperatures very little motion is observed since individual particles have a

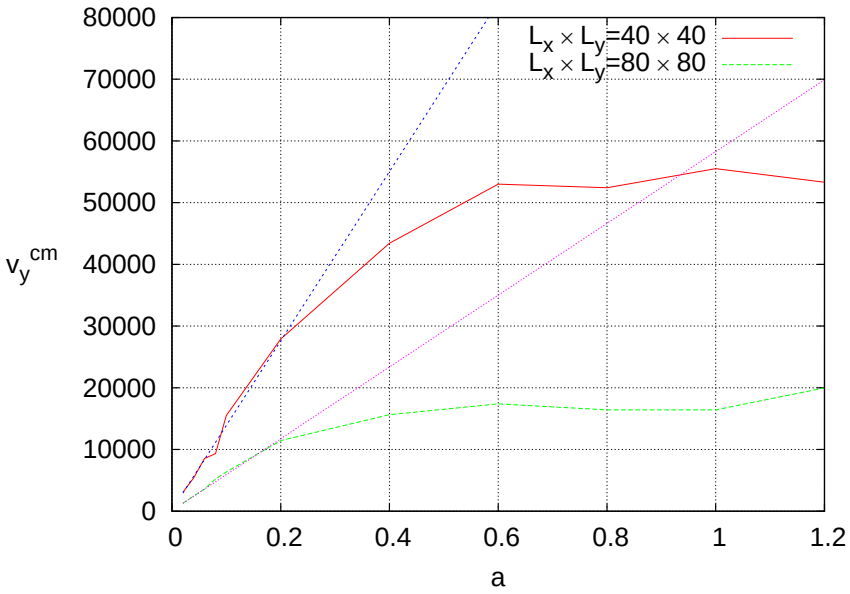

Figure 3.16: Centre-of-mass velocities in y-direction, v_y^{cm}, shown as functions of the field parameter, a. As the field is increased the velocity at which the droplet moves is increasing. When the field reaches a certain value the droplet will start breaking up into several smaller droplets. Two lines have been fitted to the lowest field values to illustrate the linear dependence between v_y^{cm} and the field, a. Δx is set to be $\Delta x = 110$.

low probability to break loose from the droplet and the droplet tends to stay at the same position throughout the simulation. The opposite happens at high temperatures. As the temperature is raised the probability of particles leaving the droplet gets higher and, if the temperature is raised further the droplet will eventually evaporate.

A short investigation of how field or step height and surface length affect the outcome of the simulation was conducted. The setup consisted of two potential drops. The middle step's length was the varied parameter. It was found that as the field is raised it becomes more likely that the droplet will start moving through diffusion. The longest step length was chosen to be $l = 60$. The length of the droplet was $L_y = 60$ and width $L_x = 180$. The droplet located initially very close to the step edge, thus removing the problem of the droplet finding the step edge. The results from these runs are presented in Table 3.5.

From the results in Table 3.5 it was concluded that to be certain to have

Table 3.5: Table indicating diffusive, D, and flow, F, motion of a droplet down the steps. The data have been taken from the simulations where the step length and height were varied. a stands for the change in field per step parameter. Temperature was $T = 0.6$.

surface length	$a =$ 0.05	$a =$ 0.06	$a =$ 0.07	$a =$ 0.08	$a =$ 0.09	$a =$ 0.10	$a =$ 0.11	$a =$ 0.12	$a =$ 0.13	$a =$ 0.14	$a =$ 0.15
5	F	F	F	F	F	F	F	F	D	D	D
10	F	F	F	F	F	F	F	F	D	D	D
15	F	F	F	F	F	F	F	F	D	D	D
20	F	F	F	F	F	F	F	D	D	D	D
25	F	F	F	F	F	F	F	D	D	D	D
30	F	F	F	F	F	F	F	D	D	D	D
35	F	F	F	F	F	F	F	F	D	D	D
40	F	F	F	F	F	F	D	D	D	D	D
45	F	F	F	F	F	F	F	D	D	D	D
50	F	F	F	F	D	F	F	F	D	D	D
55	F	F	F	F	F	F	F	F	D	D	D
60	F	D	D	D	D	D	D	D	D	D	D

Table 3.6: Table similar to Table 3.5 but here the temperature has been raised to $T = 1.0$.

step length	$a =$ 0.05	$a =$ 0.06	$a =$ 0.07	$a =$ 0.08	$a =$ 0.09	$a =$ 0.10
5	D	D	D	D	D	D
10	D	D	D	D	D	D
15	F	D	D	D	D	D
20	F	F	D	D	D	D
25	D	D	D	D	D	D
30	F	D	D	D	D	D
35	F	D	D	D	D	D
40	F	F	D	D	D	D
45	F	F	D	D	D	D
50	F	F	D	D	D	D
55	F	F	D	D	D	D
60	D	D	D	D	D	D

a system where the droplet flows down the step the step height, or field parameter, should be lower than $a = 0.1$ or even lower than $a = 0.09$. This critical a-value, above which individual particles move by diffusion and below which the droplet flows, is temperature dependent. This can be seen when comparing Table 3.5 with Table 3.6. As temperature is raised further, particles are able to break loose from the droplet, and as the field is raised, it will be less and less probable for these particles to move back up the step. Therefore to see the effect of an increased temperature on these results, some of the above simulations were run at a higher temperature.

As can be seen in Table 3.6, a slight increase in temperature will dramatically change the behaviour of the systems. If there is a need to run simulations at a higher temperature the field parameter should accordingly be lowered to avoid a diffusive system.

Summarising the observed behaviour, one can say that, to get the droplet to move as a single droplet then the temperature, field and droplet size must be in harmony. If the temperature is too high the droplet will evaporate. If it is too low then the event probability gets too low. When the field parameter is increased, single particles will tend to move over the step edge in one direction only and thus the droplet will start breaking up. A second droplet will form on the lower step, indicating the particles have diffused over the

step edge. On the other hand, if the field is too low then the droplet will move very slowly over the step edge. The size of the droplet affects the time it takes for it to move over the step edge. The time it takes for a droplet to flow over a step edge will increase with droplet size.

Once the basic mechanisms about how the parameters affect the droplet dynamics were understood the temperature was fixed to $T = 0.8$ in units per k_b. The drop was initially located symmetrically over the step edge.

The temperature $T = 0.8$ is low enough for a droplet to flow as a single unity over the step edge at most fields. When increasing the temperature the droplet will flow faster over the step edge, thus saving computation time, but also increasing the risk of having the droplet evaporate. At lower temperatures it turned out that simulations tend to suffer from insufficient precision in the used double-precision floating point numbers. The probability of a particle for completely leaving the droplet was smaller than the precision of the above mentioned floating point numbers. The result of increasing the precision was then observed as a decrease in errors. The error, which revealed itself in centre-of-mass graphs as step-like looking parts, where the y-coordinate remained constant, was clearly decreased when using higher floating point precision.

In order to eliminate variation in the starting time for translocation over the step edge, the droplet's centre-of-mass was initially placed on the step edge in all simulations. In the case of multiple steps, the step edges were located so that the first edge was aligned with the back edge and the last step with the front edge of the droplet. All other steps would then be equidistantly placed under the droplet. Systems with both one step and multiple steps located under the droplet in its initial configuration are shown in Fig. 3.6 (a) and (b).

The droplets studied in this chapter were all symmetric, i.e. the length in the x-direction was equal to the width in the y-direction. Next, the centre of mass velocity will be studied as a function of various droplet side lengths and the droplet will be placed on a lattice so that all steps will be under it.

3.7 Droplet motion dependence on step lengths

Previously, in Section 1.4, it was mentioned that droplet filters might be constructed so that they allowed only droplets of certain size to move large distances on a substrate.

Table 3.7: Measured times for droplets to completely translocate to the second surface after finding the second step edge.

step length, Δs	40	50	60	70	80	90	100	110	120
$\Delta t \times 10^2$	0	0	0	0,9	1,82	4,8	-	-	-

The idea behind these filters is to have at least two step edges, and let the droplet attempt to move over the step between these two edges. After having moved over the first edge, the droplet will not find the second within reasonable time, if the step is too long.

This idea was tested by simulating systems containing two step edges and an equilibrated 80×80 large droplet. The middle step's length was varied in the range of 40 to 120 lattice sites.

Table 3.7 shows the times, as functions of the middle step length, it took for the droplets to reach the second step edge once they had passed the first. The times are the real times calculated from the probabilities of the made moves. The time for a move to occur is calculated from Eq. (2.16) in Section 2.4.

The droplet finds the second step edge immediately in the case of the three shortest steps, whereas it never finds it in the case of the three longest middle-steps. Due to collective diffusion all droplets eventually find the second step edge. In these simulations this never occurred. The simulations were allowed to run about ten times longer than what it requires for the droplet to find the second step edge on a step 90 lattice sites long.

In Fig. 3.17 is shown a droplet that did not find the second step edge during a simulation. The droplet is randomly moving around between the steps but this random motion is very slow. If the droplet is given enough time, it will eventually find the lowest step and move over it.

Next in this section we will have a closer look at the random motion of the droplet and also at how the individual particles inside of it move. In other words, we study the collective and tracer diffusion of the droplet. The collective diffusion describes how the droplet moves as a whole, whereas the tracer diffusion looks at the motion of individual particles. We expect large differences between the collective and tracer diffusion. The droplet moves very slowly compared to how many moves are made in a typical simulation, therefore the tracer diffusion is expected to be much larger than the collective diffusion.

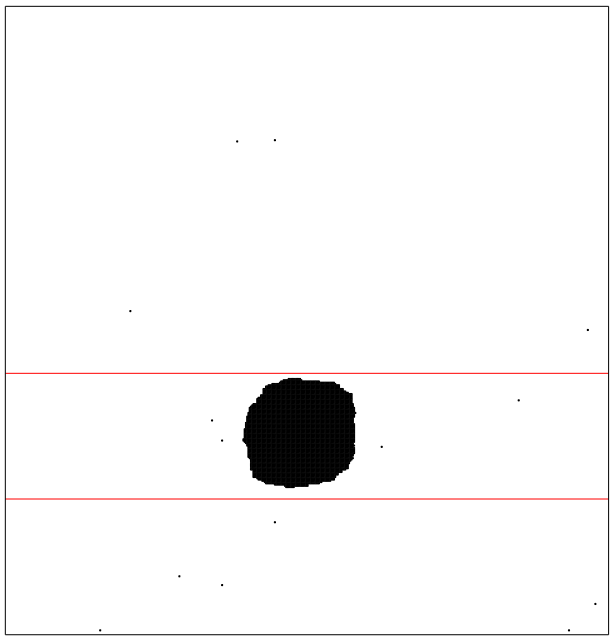

Figure 3.17: Droplet in a simulation where it did not find the second step edge. In this case the distance between the first and second step edge was 100 lattice sites. In this picture the field decreases downward, in other words the droplet would be moving down. The red lines indicate the step edge boundaries.

The collective diffusion is calculated from

$$D = \frac{1}{N} \sum_{i=1}^{N} \frac{d_{i,x}^2 + d_{i,y}^2}{t_i - t_{i-1}}, \tag{3.5}$$

where $\vec{d_i} = \vec{r_i} - \vec{r}_{i-1}$ is the distance moved between two samples, $\vec{r_i}$ is the centre-of-mass coordinates at time i , $t_i - t_{i-1}$ is the time between the two outputs i and $i-1$ and N is the number of outputs. The tracer diffusion is calculated from

$$D = \frac{1}{N} \sum_{i=1}^{N} \frac{d^2}{\tau_i} = \frac{1}{N} \sum_{i=1}^{N} \frac{1}{\tau_i}, \tag{3.6}$$

where τ_i is the time needed to move one particle during the i:th update of the algorithm. In Eq. (3.6) we have $d^2 = 1$ since any given particle is only allowed to move to a neighbouring site in either x- or y-direction.

In Figs. 3.18 (a) and (b) both the collective and tracer diffusion are plotted for square droplets with side lengths L=20, L=40, L=80 and L=100. The difference between these two types of diffusion can be seen from the steady state values. The difference is on the order ten decades.

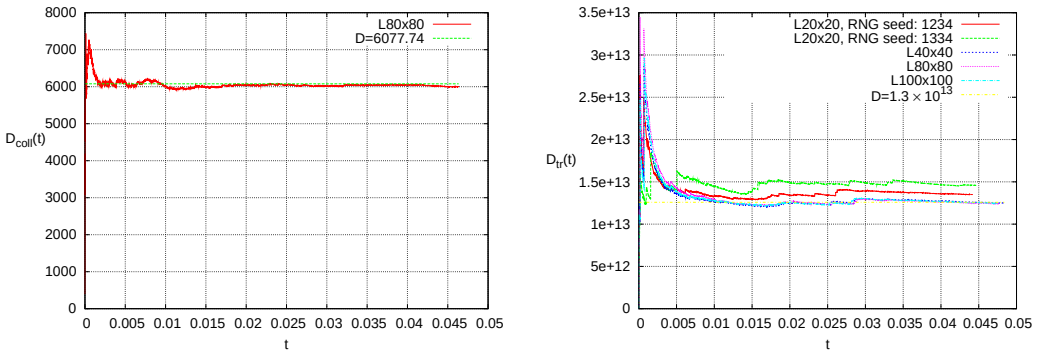

(a) **(b)**

Figure 3.18: **(a)** Collective diffusion, D_{coll}, plotted as function time, t. The system shown here has the size $L_x = L_y = 80$. **(b)** Tracer diffusion, D_{tr}, plotted as a function of time, t, for various system sizes. The jaggedness that appear at the same moments of time was checked to be an artifact from the random number sequence by running one system with a different set of random numbers.

The vastly greater tracer diffusion values, compared to the collective diffusion, confirms that the dynamics of particles inside the droplet is extremely fast compared with the collective droplet motion. The conformational change towards equilibrium configuration is seen at short times.

In Fig. 3.19 the logarithms of the diffusion constants are plotted as functions of the droplet's side length. We see that small droplets move about considerably faster than larger ones, while the tracer diffusion constant is independent of the droplet's size.

In Fig. 3.20 we have plotted the quotient of the tracer diffusion divided by the collective diffusion as a function of time for the $L = 80$ system. We see from these plots that the movement of the individual particles is considerably greater than the movement of the entire droplet.

In Fig. 3.18 (b) we notice an interesting phenomena. The graphs for the four systems appears to show the same jaggedness at roughly the same time values. We assumed this was an artifact from the fact that we are using the same random number sequences in these four cases. To check this a system of the size $L = 20$ was rerun using a different random number seed, the result

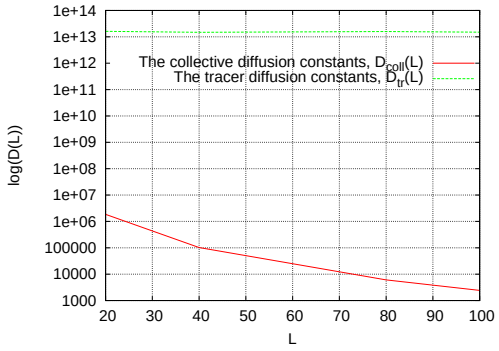

Figure 3.19: The logarithm of the diffusion constants, $\log(D)$, plotted as a function of the droplets' side length, L.

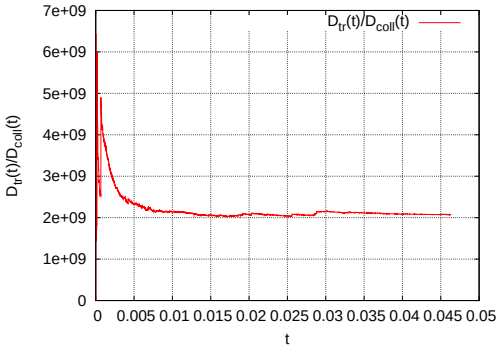

Figure 3.20: The tracer diffusion divided by the collective diffusion, D_{tr}/D_{coll}, plotted as a function of time.

was that the jaggedness no longer appeared in the same locations.

3.8 Centre-of-mass velocity saturation of free and periodic droplets on a substrate with multiple steps

We will first look at how multiple steps affect the motion of the droplet in periodic and non-periodic systems. After this we will look at how the starting position in non-periodic systems affects the centre-of-mass velocities.

The systems compared here contained droplets of size $L_x \times L_y = 80 \times 80$ and were simulated at identical fields. The only difference is that one is periodic the other is not. The centre-of-mass velocities for the non-periodic and the periodic systems are shown in Figs. 3.21 (a) and (b).

The centre-of-mass velocities saturate as we increase the field for the system with only one step edge. But when we also increase the number of steps we notice we are able to transfer the particles quicker across the step edges.

Next we will look at how the droplet's initial location affects the outcome of the simulation. The system size was 80×80 and the droplet was initially located on top of the step edge(s). A second set of simulations, where the droplet was initially located on the first surface, was also run. The reason for placing the droplets like this was to find the critical field value at which the droplet breaks up into two or more partitions.

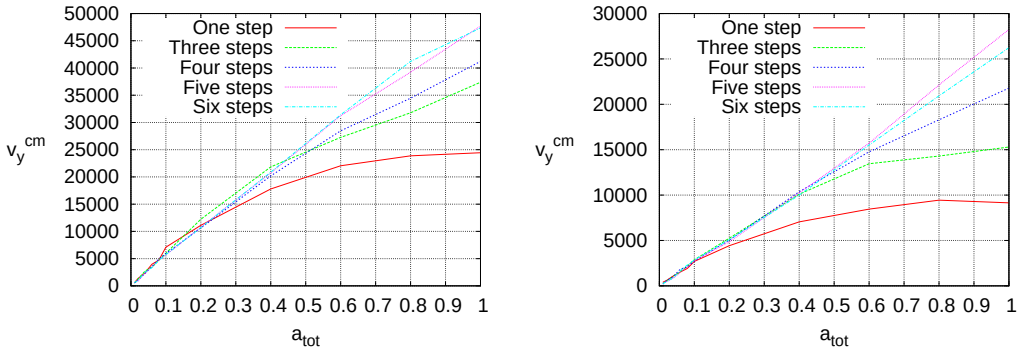

Figure 3.21: **(a)** Free droplet centre-of-mass velocities in y-direction, v_y^{cm}, plotted as functions of the total field difference, a_{tot}, between the first and the last surface. **(b)** Periodic droplet. We see the same dependence on a_{tot} as in (a), namely, by increasing the number of steps we are able to transfer the droplet faster.

At first, a system with one step was simulated at field values both below and well above the field that was earlier found to cause the droplet to break up as it moved over the step. Then a system with five steps was simulated and the same was checked there, too. In other words, the question addressed with these simulations is: when does the droplet break up and start moving over the step diffusely and how does adding more steps affect this? Both cases for initial droplet locations were investigated yielding some interesting results.

It was found that the droplet breaks up at nearly the same total field difference between the first and the last step for the one and multiple step configurations. The droplet was initially on the first surface, as illustrated in Fig. 3.22 (a). The droplet was found to break up at the field $a \approx 0.16$ for the one step system. For the system with multiple steps it broke up when the field change per step was $a \approx 0.04$. The field at which the droplet breaks up was found by looking at snapshots from the simulations.

The observation that a_{tot} determines v_y^{cm} regardless of how many partial fields it is divided into indicates two things. First, random diffusion of holes inside the droplet is not significant at those step lengths, and, secondly, that the droplet's change in form does not affect translocation significantly even in the case of multiple steps. This is in line with the observation that the droplet equilibration is slow compared with its translocation, see Section 3.5.

The other type of system that was simulated was for a droplet that had all steps located underneath it in its initial position, see Fig. 3.22 (b). It was

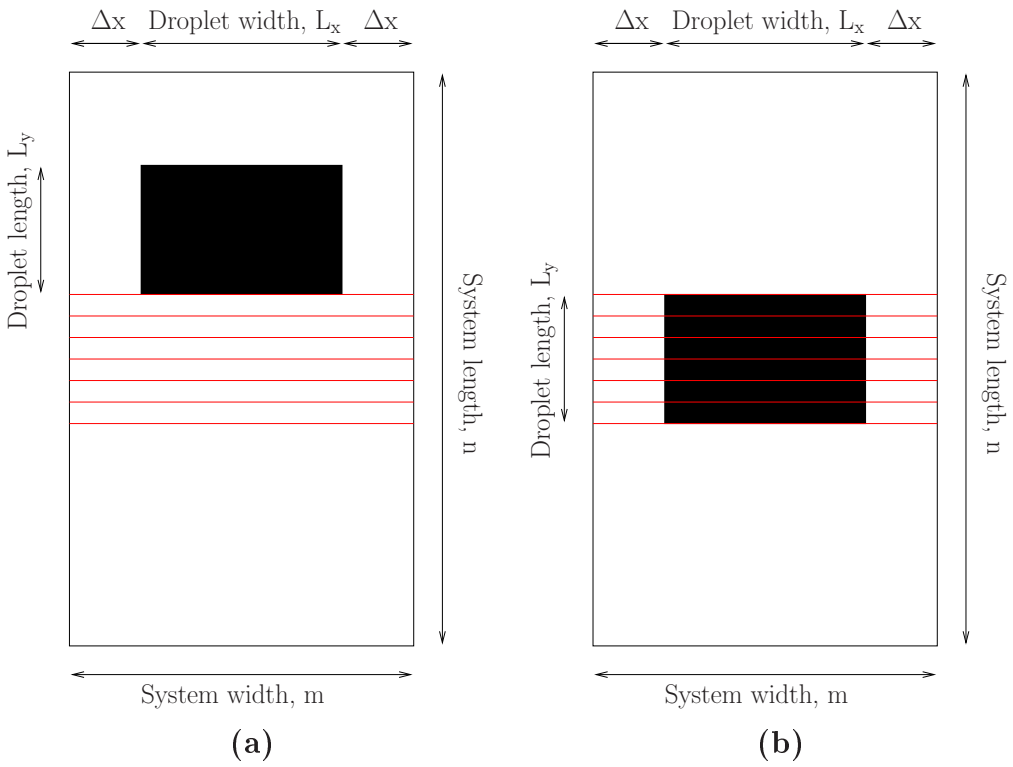

Figure 3.22: Systems in their initial configurations. **(a)** The droplet is located entirely on the first terrace, or surface. **(b)** All step edges are located under the droplet. The red lines indicate where the step edges are with respect to the droplet's initial location.

found that no matter how high the field was made, the droplet would not break up, but the velocity would saturate instead. The saturation field was found to be higher than the field needed to produce single-particle diffusion in systems like the one in Fig. 3.22 (a).

Next, velocities for the latter system, see Fig. 3.22 (b), were compared. The sample systems contained one and five steps, and it was again found that the relevant parameter is the total field between the first and last step the droplet comes into contact with. In this case, the total field change determines how fast the droplet will move over the steps. In Table 3.8 the velocities from the four systems are compared using $a_{tot} = 0.04$ and $a_{tot} = 0.08$. The velocities at which the droplets move are very close to each other, confirming that at fields smaller than the value at which the velocity saturates the total field difference between the first and the last step determines their velocity.

For systems with multiple steps, like the one in Fig. 3.22 (b) the first edge is neglected when calculating the total field difference between the first and the last steps. This is due to the initial location of the droplet. In the initial configuration the droplet's back edge is aligned with the first step edge. Once the simulation is started the droplet will start moving away from the first step.

Table 3.8: Velocities for free droplet systems with one and fives steps. The velocities are measured in the beginning of each simulation. The systems are of the same type as the one in Fig. 3.22 (b).

	$a_{tot} = 0.04$	$a_{tot} = 0.08$
One step	2390	4680
Five steps	2370	4780

When the field is raised above the field for saturation, the droplets will no longer move with the same velocity. The saturation field was found to be in the proximity of $a = 0.4$ for a system with a non-periodic droplet initially over the step edges as in Fig. 3.22 (b). Similarly the saturation field for the five-step system was found to be near $a = 0.4$, where a refers to the field-change per step.

In Fig. 3.23 centre-of-mass velocities are plotted as functions of field-change per step for non-periodic systems. The graphs in Figs. 3.23 (a) and (b) were obtained for simulations starting from initial configurations depicted in Figs. 3.22 (a) and (b), respectively. We see from these graphs that by introducing more steps we are actually able to increase the saturation velocity for both setups. We also tried to find the critical field for when the droplet splits and starts moving through driven diffusion for the system depicted in Fig. 3.22 (b). Surprisingly enough, we found that the droplet never breaks up.

The centre-of-mass velocity saturation can be explained using the same argument as in Section 3.3 for the centre-of-mass saturation for periodic droplets. In that section we looked at how raising the field influences the amount of particles, and holes, that move over the step edge in a periodic system.

As long as the field is low, particles are able to move over the step edge in both directions. As we raise the field we limit the single particle movement to the upper step once they have reached the lower step. For systems where the droplet is located initially on the upper step this means the individual particles will move through diffusion to the lower step. In Fig. 3.3 we see

that the **none** ↔ **none** mode becomes the most active as the field is raised. At low fields it is almost as active as the **all** ↔ **all** mode, since particles are able to move over the step edge in both directions.

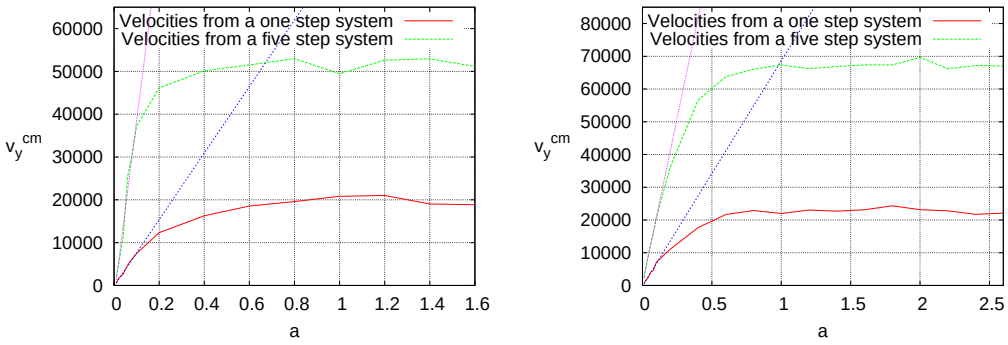

Figure 3.23: Centre-of-mass velocities, v_y^{cm}, as functions of field per step edge, a. **(a)** The initial configuration as depicted in Fig. 3.22 (a). **(b)** The initial configuration as in Fig. 3.22 (b).

The particle moves that cause the droplet to move over a step edge were found very similar between the one step edge and the five step edge case. Modes obtained for a system with one step edge and with five step edges are shown in Fig. 3.24 (a) and (b). The field change per step edge $a = 0.06$. The modes for the five step system were measured over the last step edge.

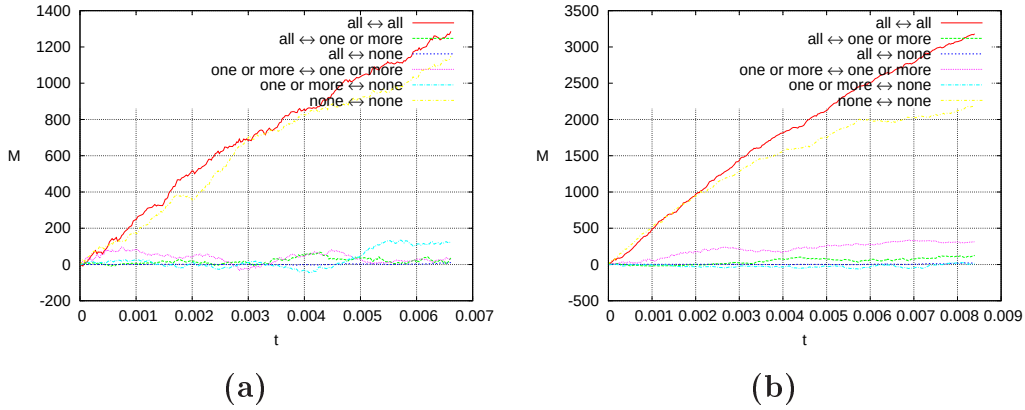

Figure 3.24: Modes of movement, M, as function of time, t, taken from a system with **(a)** one step edge and **(b)** five step edges. The modes shown here were observed on the last step edge. Field change per step is $a = 0.06$.

In both cases the dominating modes are **all** ↔ **all** and **none** ↔ **none**, which

correspond to particles moving inside the droplet and single particles moving outside the droplet. A more thorough discussion of how the modes depend on the field is given in Section 3.1.

A practical implementation of these results could be used to overcome the maximum velocity limit of a droplet translocated over a surface, inherent to the one-step edge system.

3.9 Centre-of-mass velocity dependence on the length of the droplet in non-periodic systems

In Chapter 3.2 we looked at how a periodic droplet's centre-of-mass velocity depends on its length. Using the data from those simulations we were able to verify the method we use in these simulations to produce correct results.

In this chapter we will look at how the centre-of-mass velocity depends on the length of a free droplet and also discuss the observed differences.

Systems of sizes 80×80, 80×100, 80×120, 80×140, and 80×160 were studied. The velocities, shown in Table 3.9, have been averaged over five iterations.

Table 3.9: Velocities for free droplets with sizes $(L_x \times L_y)$ 80×80, 80×100, 80×120, 80×140 and 80×160. The velocities have been averaged over five iterations.

velocity	$L_y = 80$	$L_y = 100$	$L_y = 120$	$L_y = 140$	$L_y = 160$
mean	7433.8	7042.3	5649.9	5482.1	5024.9
stddev	150.05	189.44	238.94	163.46	189.44

In Fig. 3.25 the velocities are plotted as functions of the droplets' length. The function $f(x) \sim 1/L_y$ is fitted to the data.

The fitted function, that was found to describe the velocity dependence on droplet length, for periodic droplets, does not work for free droplets. The differences to periodic droplet translocation, Fig. 3.8, comes from the droplet being able to deform in the x-direction and moving over the step edge using modes other than only the **all** $\leftrightarrow$ **all** mode. The modes that are active in a non-periodic system are shown in Fig. 3.26 (a). At lower fields we see an

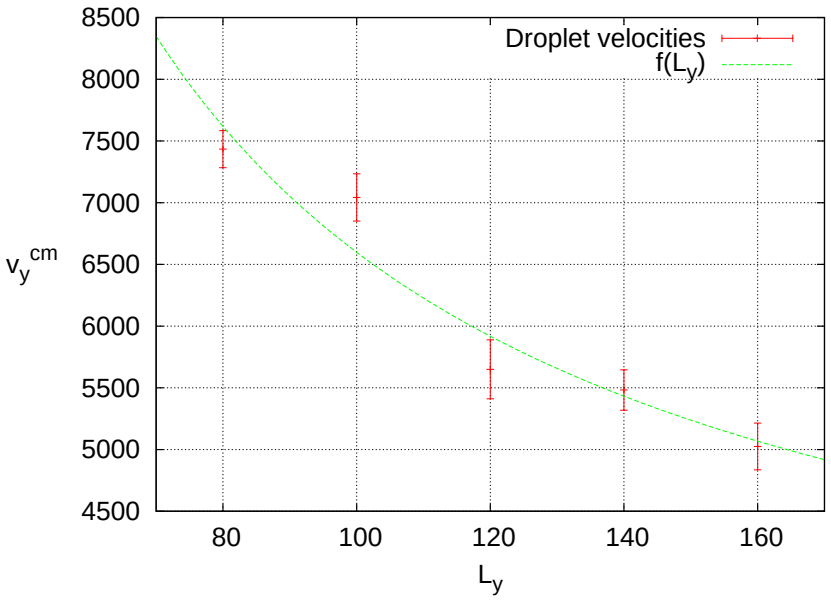

Figure 3.25: Centre-of-mass velocities, v_y^{cm}, plotted as functions of the droplet length, L_y. The velocity data used for this plot is shown in Table 3.9. The function $f(x)$ has the form $f(x) \sim 1/x$.

increase in the modes that stayed close to zero in Fig. 3.26 (a). The mode **one or more** $\leftrightarrow$ **one or more** shows a significant increase. A system at $a = 0.01$ is shown in Fig. 3.26 (b).

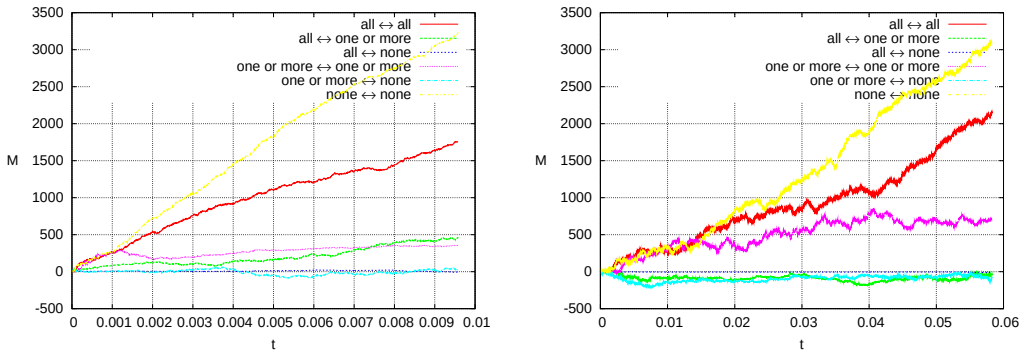

(a) **(b)**

Figure 3.26: Modes, M, plotted as a function of time, t. The data was collected by counting how many particles belonging to each mode moves over a step edge. A non periodic system with a 80×80 large droplet at **(a)** field $a = 0.1$. **(b)** Field $a = 0.01$.

3.10 Droplet motion using triangular field

A triangular field was used to study whether the droplet velocity could be further increased. The triangle was chosen to open up in the same direction as the droplet was moving in. The reason for constructing the field this way was that once the droplet starts moving over the field it should stick together at higher fields. This is due to the droplet being squeezed into the tip of the triangle instead of being evenly pulled over the step as with a straight step edge.

Fig. 3.27 depicts a typical system. Basically, the field would start from the middle of the simulation lattice and extend so that the legs of the triangle have the same coordinates as the two lower corners of the lattice. The droplet would be placed sightly on top of the tip of the triangle. As was to be expected, the time required for the droplet to find the tip is even longer than what is required for it to find a straight step edge. Due to this the droplet was placed slightly on top of the tip.

Before letting the droplets translocate they were equilibrated to avoid effects from changes in the droplet form. These changes are likely to be more significant with the triangular than with straight step edges.

The remarkable thing noticed in the simulations was that no matter how high the field is, the droplet does not break up. Centre-of-mass data for the largest droplet and all particles on the simulation lattice are plotted together in the same graph in Fig. 3.28. Since the centre-of-mass graphs for simulations with the same field fall nearly perfectly on top of each other it was concluded that the droplets do not break up and in fact stay as single large droplets throughout the simulations. This is in dramatic contrast with a straight step edge system for which the critical field, at which the droplet starts breaking up, is close to $a = 0.16$.

The observations made above go to show that by simple geometric modifications droplet translocation can be dramatically affected.

3.11 Metropolis simulations

Some systems have been simulated using the Metropolis method in order to make a comparison between this traditional method and the N-fold way. From the results a correction to the time constant, τ, can be calculated.

The actual τ value can be used to evaluate how long a simulation utilising the

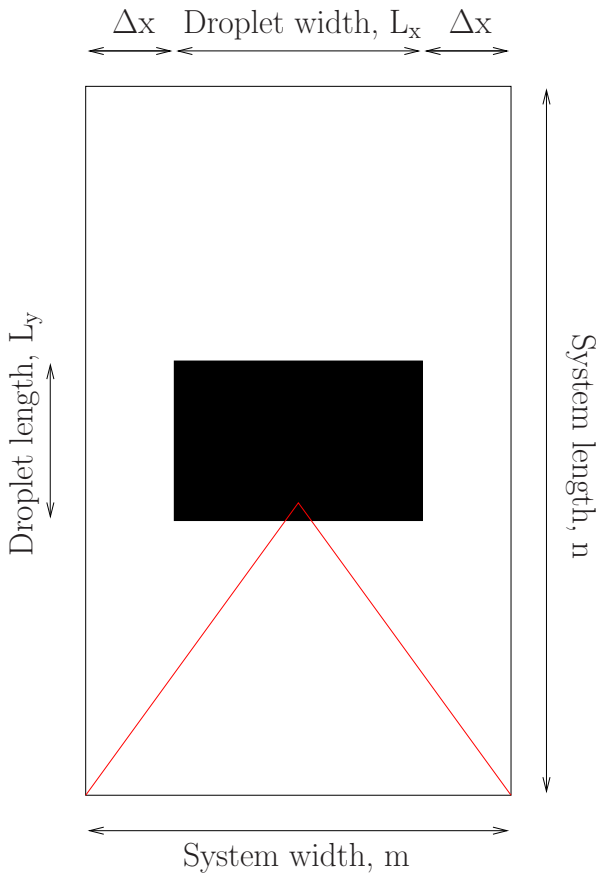

Figure 3.27: Typical setup of a system using a triangular field. The droplet is placed so that it overlaps the tip of the triangle, this way the time needed before the droplet starts moving over the edge is greatly reduced.

N-fold way method would have taken, had it been run with the Metropolis method.

The systems simulated using the Metropolis method have been quite limited in size due to the time needed to simulate systems at low temperatures. A system simulated using the N-fold way method was normally of the size of several hundreds of particles long and wide. The temperature used in all N-fold way and Metropolis simulations was fixed to $T = 1.0$. The temperature was $T = 0.8$ in previous simulations using the N-fold way methods, but here it was raised to $T = 1.0$ to speed up the droplet dynamics in the Metropolis simulation. The size of the droplet is also limited to only $L_x \times L_y = 60 \times 60$.

Only the part of the centre-of-mass graphs where the droplet moves ballisti-

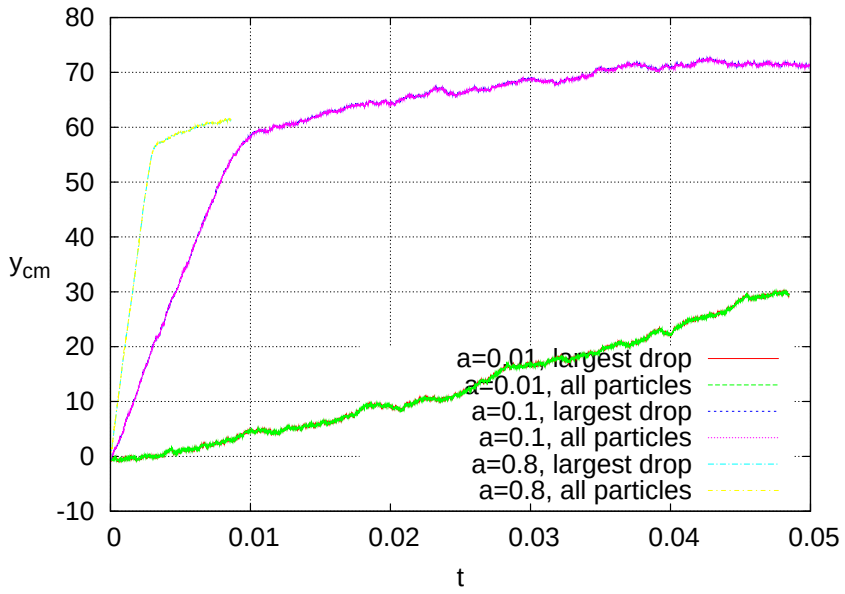

Figure 3.28: Centre-of-mass data, y_{cm}, as a function of time, t, calculated using all particles. Only those in the largest droplet are plotted in the same graph. Data for the largest droplet have been obtained using the Hoshen-Kopelman algorithm described in Section 2.6. In Fig. 3.29 there is a closer look at the two graphs at the lowest field, $a = 0.01$.

cally has been used when calculating the correction to τ used in the N-fold way method.

The field parameters were $a = 0.2$, $a = 0.4$, $a = 0.6$, and $a = 0.8$. The corrections to τ obtained from these systems are shown in Table 3.10.

The τ value used in all simulations was fixed to $\tau = 10^{-10}$. Factoring in the correction, τ_c, we obtain the $\tau_{N\text{-fold}}$ value that will make the N-fold simulations produce measurables on a time scale similar to what a corresponding Metropolis simulation would have produced.

Table 3.10: Corrections to the time constant, τ, in the N-fold way method obtained from comparing Metropolis to N-fold way simulations.

Field, a	0.02	0.04	0.06	0.08
τ_c	2.3×10^{10}	2.4×10^{10}	2.0×10^{10}	2.2×10^{10}

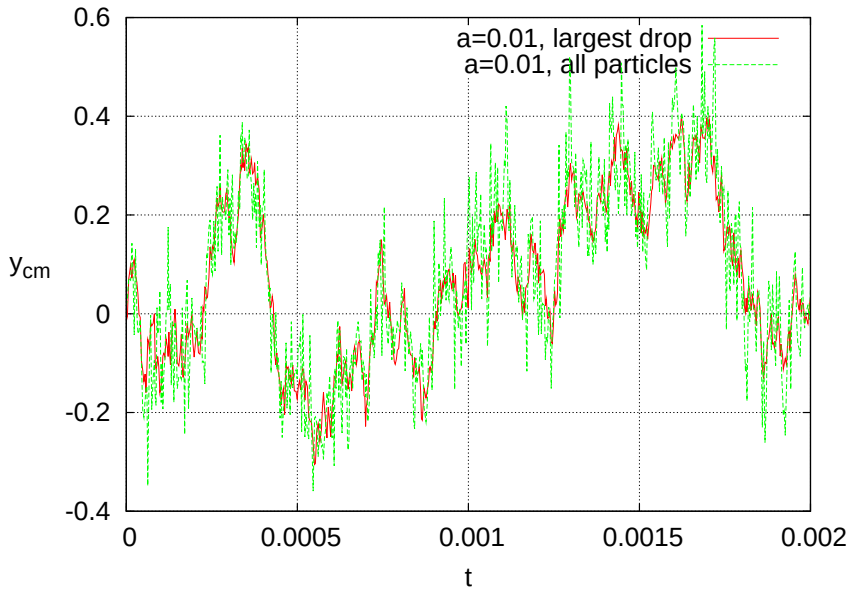

Figure 3.29: A closer look at the centre-of-mass data, y_{cm}, as a function of time, t, obtained from the simulation at the lowest field, $a = 0.01$. Here it can be seen how the two data sets fall on top of each other. The data set that only contains data from the largest droplet appears to be much smoother than the other. This is due to particles being tightly bound to the droplet whereas in the other case there might be free particles moving around on the simulated lattice.

As a comparison, shown in Fig. 3.30 there are two systems, one simulated using the Metropolis method and one using the N-fold way method. The N-fold way data have been scaled using the correction coefficients found from the previous simulations. These two methods for simulating Ising systems, shown in Fig. 3.30, produce similar results. The data in this figure have been collected from the system's largest droplet using the Hoshen-Koppelman method, described in Section 2.6.

The time data from the Metropolis method was measured in numbers of Monte Carlo time steps. One Monte Carlo time step corresponds to N updates of the algorithm. $N = L_x \times L_y$ is the total number of lattice sites on the lattice. In summary, the correspondence between N-fold and Metropolis time is reasonably good showing slight field dependence.

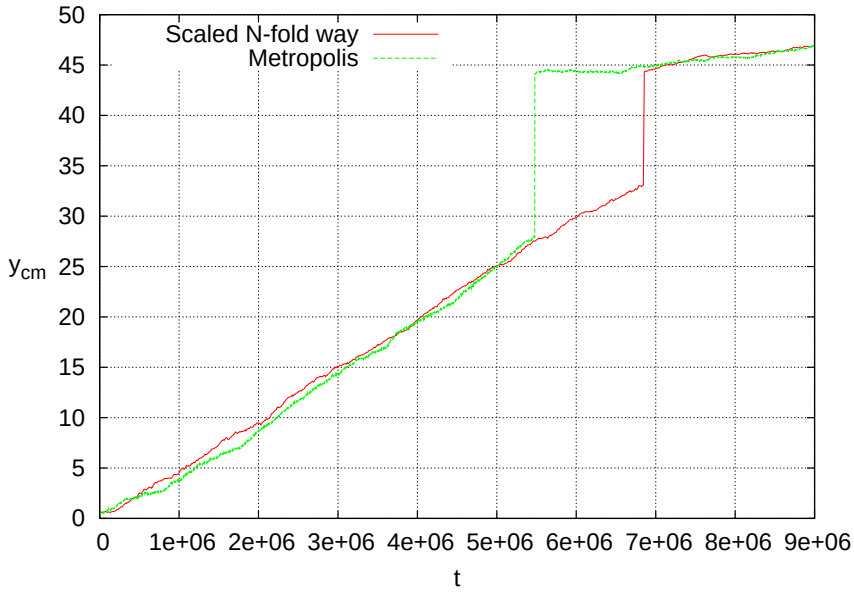

Figure 3.30: The same system has been simulated using both the Metropolis and the N-fold way method. The centre-of-mass data, y_{cm}, from the N-fold way method have been scaled to produce the same time, t, dependence as the data from the Metropolis method.

3.12 Finite size scaling analysis

In this section we will look at how the different system sizes depend on the field parameter and the size of droplet. Our objective is to investigate universal features in the ballistic and diffusive transport over a step edge. To do this we develop a method to calculate the probability of a droplet to break as it translates over a step edge. We will then attempt to achieve a data collapse for all systems sizes once we know how the probability for a specific system depends on the droplet size.

The tricky part in our system is that it is anisotropic, which in our case is due to the driving field acting differently in the x- and y-directions This, in turn, is reflected e.g. on the form and dynamics of the droplet. There have been studies of anisotropic systems in the past [44, 45].

3.12.1 Order parameter for finite size scaling

Initially we wanted to base our finite-size scaling analysis on the behaviour of the modes of the system calculated at a step-edge.

In Fig. 3.26 we compared the same droplet simulated at different fields. We see here that different modes are active at high and low fields. As soon as the droplet breaks up only one mode is active, namely the **none** $\leftrightarrow$ **none** mode. Hence, we used the assumption that at low fields the ballistic and diffusive modes will be of similar magnitude while at higher fields the diffusive mode will dominate. We calculated the probability for the droplet to stay together from

$$\Pi \sim \frac{M_{ballistic}}{M_{ballistic} + M_{diffusive}}.$$

We found that the probabilities obtained using this method did not differ much from each other, regardless of whether the droplet stayed together or not. Therefore another method for calculating the probability for splitting was needed.

The second method we tried is based entirely on the geometry of the system. We calculate the time when the droplet splits, t_{split}, and normalise it with the total time it takes for all particles to translocate to the lower step, t_{total}. The probability is now obtained from

$$\Pi \sim \frac{t_{split}}{t_{total}}.$$

Using the latter method we were able to obtain a data collapse. The anisotropy of the studied Ising system presents problems to finite-size-scaling analysis. We first present reasonable data collapses when varying the linear dimensions L_x and L_y separately. Then we combine these procedures to find the field parameter fixed point and obtain the true droplet size scaling in its vicinity.

3.12.2 Finite-size scaling with respect to the droplet width

The data used in this analysis was collected from systems with widths ranging from $L_x = 40$ to $L_x = 160$. The field parameter was systematically varied between $a = 0.02$ and $a = 2.0$. The temperature was kept constant at $T = 0.8$.

Table 3.11: Critical field values for when the probability to split into two droplets, $\Pi\left(a = a_c\left(L_x\right), L_x\right)$, is 0.5.

Droplet size, L_x	40	80	120	160
Field, a_c	0.335	0.206	0.203	0.182

The finite size scaling analysis done here studies the droplet splitting. First, a scaling function $\Pi\left(a, L_x\right)$ is defined. It gives the probability for the droplet to split into several droplets as a function of the field parameter a.

Now the critical field is defined as the field at which the probability of the droplet to split is $\Pi\left(a = a_c\left(L_x\right), L_x\right) = \frac{1}{2}$. (The word critical should be understood in a loose sense, since we are analysing dynamic not thermodynamic transitions.) The critical field values, a_c, are shown in Table 3.11 for the four systems.

In Fig. 3.31 (a) data from these simulations are plotted according to Eq. (3.7). By setting the scaling constant as $\nu = 0.4 \pm 0.05$ we are able to obtain a data collapse.

$$\hat{\Pi}\left(a, L_x\right) = \Pi\left(\left(a - a_c\left(L_x\right)\right) L_x^{\nu}, L_x\right). \tag{3.7}$$

The error in the parameter ν was estimated to be $\Delta\nu = 0.05$. The magnitude of the error in ν was found by slightly varying ν until a noticeable deterioration in the data collapse compared to the one for $\nu = 0.4$ was visible.

3.12.3 Finite size scaling with respect to the droplet length

The difference between the analysis in the previous section and the one here is that the parameter L_x^{ν} is replaced by L_y^{η}, in other words,

$$\hat{\Pi}\left(a, L_y\right) = \Pi\left(\left(a - a_c\left(L_y\right)\right) L_y^{\eta}, L_y\right). \tag{3.8}$$

From the simulations we obtain $\eta = 0.15 \pm 0.05$ for the parameter η. The correspondingly collapsed data are shown in Fig. 3.31 (b).

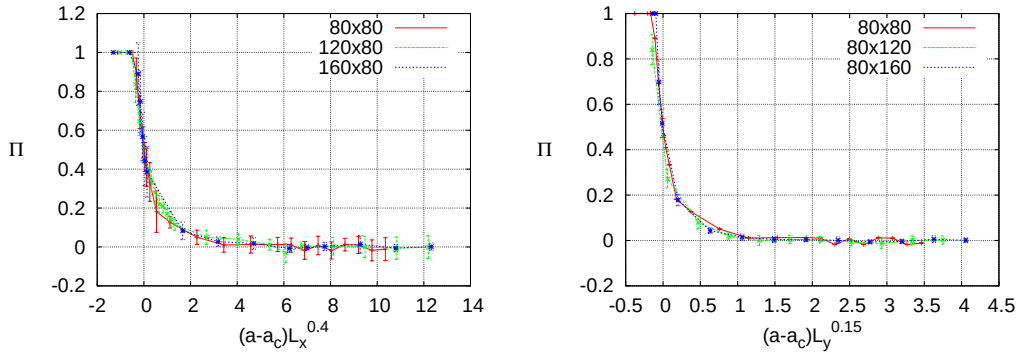

Figure 3.31: **(a)** Systems with width ranging from 40 to 160 are scaled and plotted together. By choosing $\nu = 0.4$ in Eq. (3.7) data collapse of the three different system sizes is observed. **(b)** Data collapse is achieved by keeping the droplet length constant and by choosing $\eta = 0.15 \pm 0.05$ in Eq. (3.8).

3.12.4 An isotropic finite size scaling

The complete anisotropic finite size scaling is constructed by combining Eqs. (3.7) and (3.8). Thus we get

$$\hat{\Pi}\left(a, L_x, L_y\right) = \Pi\left(\left(a - a_c\left(L_x, L_y\right)\right) L_x^{\nu} L_y^{\eta}, L_x, L_y\right). \tag{3.9}$$

We can now combine the data for systems with a fixed droplet width with those with a fixed length. Using the values for ν and η found in Sections 3.12.2 and 3.12.3 we now get the graph in Fig. 3.32.

Interestingly, even though the velocity for the ballistic transport of the droplet is much more heavily dependent on its length than width, the droplet splitting is much more significantly affected by its width.

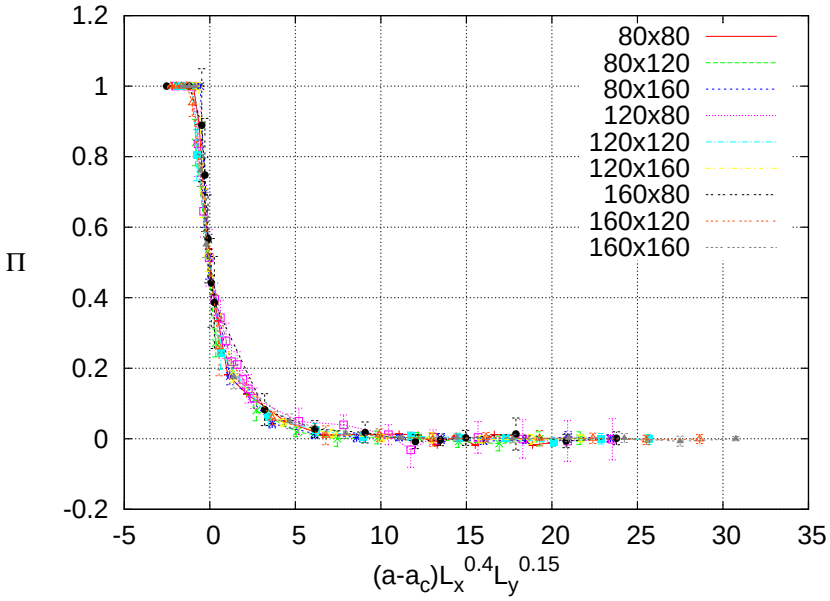

Figure 3.32: The data in Fig. 3.31 are plotted together.

Chapter 4

Conclusions

We started investigating how a droplet moves over a step by determining the dominating mechanisms. We defined modes of motion by how many neighbours a particle has before and after completing a move.

We found that in all cases the so called **all** $\leftrightarrow$ **all** mode is very active. This mode represents particles that have maximum number of neighbours both before and after a move. The **none** $\leftrightarrow$ **none** mode was found to also have a strong influence in non-periodic systems. This mode represents particles that have no neighbouring particles neither before nor after a move. For periodic systems we expected, and also found, that only the **all** $\leftrightarrow$ **all** mode is the most significant mode.

We did a simple test to verify that our simulation software worked properly. For a small periodic system we expect to have a constant transfer of mass across the step edge, which implies that the centre-of-mass velocity depends on the system length as $v_y^{cm} \sim 1/L_y$. We checked this by measuring the centre-of-mass velocity for systems containing small droplets.

We characterised the timescales of the hole dynamics with respect to the droplet translocation velocity by determining the length scale beyond which the hole dynamics starts deviating the centre-of-mass from the $v_y^{cm} \sim 1/L_y$ behaviour. We found this length scale to be roughly 200 lattice units corresponding to the simulation time-scale of order 0.8. We found evidence of the holes being mainly responsible for this velocity saturation. The holes act as random walkers inside the droplet. Therefore as we make the droplet longer it will take longer for them to reach the step edge from the lower step to accommodate for mass transfer.

Next we studied the centre-of-mass velocity as a function of the field param-

eter for periodic droplets. We found v_y^{cm} to saturate as we raised the field. This is understandable by considering the step edge as a probability barrier. The higher the field, the lower is the probability for a particle to move over it so that it increases its energy. At low fields there is a constant flow of particles (and holes) that are moving over the edge in both directions. At low fields we found the centre-of-mass velocity to linearly depend on the used field parameter, a.

After having verified the model and identified which processes drive periodic droplets over a step edge we focused on non-periodic, or free, droplets. First we determined the role of individual particles crossing the step edge outside of the droplet. This we did by investigating how the droplet width subtracted from system width affect the motion of the droplet. We found that the finite size width of the system no longer affects the results if the distance on either side of the droplet to the sides of the system is greater than $\Delta x \geq 100$.

Once we had determined the required size of our non-periodic system we set out to describe the centre-of-mass velocity dependence as a function of the field parameter. We again found that at low fields we have a linear dependence while at higher fields saturation is observed. Whether the droplet splits or moves as a whole over the step edge is highly dependent on its starting location, unlike for periodic droplets. The droplet initially located entirely on the first surface was found to split for fields above a critical value. The droplets were much more resilient to splitting if they resided initially over the step edge.

Next we studied how step length and temperature affects the way the droplet moves. Quite expectedly, we found that making the steps longer and raising the field will increase the probability for the particles to decouple from the droplet and move diffusively. Increasing the temperature was also verified to increase this probability, as it should. Based on these results, we briefly studied the possibility of constructing a droplet filter.

The droplet filter can block the transfer of droplets smaller than some particular size. This can be done by using a system with two step edges and choosing the field low enough, so the droplet will move ballistically. The time it takes for droplets to find the second edge depends on the length of the surface between the two edges. The shorter this step, the more likely it is for a droplet to quickly find the second edge and traverse over it. By measuring the tracer and collective diffusion constants for the systems, we found that the collective droplet diffusion on a surface is extremely slow compared to particle diffusion and ballistic motion of the droplet. Hence, the distance beyond which the droplet does not find the step edge at time scales relevant

to ballistic transport are of the order of a couple of lattice units. This enables one to define very precisely the minimum size for droplets which can pass over the step.

Having more than one step edge in the system was also found to speed up the droplet as it moved over the step edges. This was observed both for periodic and non-periodic systems. For non-periodic systems we also found that the initial location of the droplet with respect to the edges influence how it will move over them. We were not able to break up the droplet by increasing the field if the droplet was located initially with the steps under it. On the other hand, if the droplet was initially located away from the step edges, breaking up was observed at a critical field value, a_c. We found that the droplet will tend to break up if the total field value between the first and the last surface is the same as a_c in the one step system. The droplet velocity was found to be solely determined by the total field difference between the first and the last step and not to depend on the number of steps. By increasing the number of evenly spaced step edges the droplet could be transferred across a surface apparently over arbitrarily long distances, which has significance for applications.

We already verified for periodic systems that $v_y^{cm} \sim 1/L_y$ using small droplets. For non-periodic droplets we found this observation to no longer hold. The reason for this is that in non-periodic systems all modes play a role. For periodic systems we observed a deviation from this dependence when using very long droplets. A similar study using non-periodic droplets is not possible since long non-periodic droplets tend to break early in the simulation.

Triangular fields were tested as a method for speeding up the droplet centre-of-mass velocity. Somewhat unexpectedly, it was found that the droplet velocity could be increased limitlessly by increasing the field without breaking the droplet. The droplet's being squeezed into the tip of the triangle seems to a very effective way to prevent its breakage, which also has applicative potential.

We also compared a simulation using the N-fold way method to one using the Metropolis method. We found that if the time-scaling constant, τ, in the N-fold way method is of the magnitude $\tau \sim 10^0$ then it will have a similar time-scale as the Metropolis method.

A finite-size-scaling analysis of the non-periodic droplet was performed to extract possible universality in the droplet motion. The droplet's linear dimensions were scaled individually due to the anisotropicity in the system arising from the step edge which acts as a driving force in a single direction. The probability for the droplet to break during translocation was found to

scale as $L_x^{\nu} L_y^{\eta}$, where L_x and L_y are the droplet width and length, respectively, and the scaling exponents are $\nu = 0.4 \pm 0.05$ and $\eta = 0.15 \pm 0.05$. Hence, two-dimensional droplet translocation over a step edge shows universal behaviour and has a driving field fixed point that determines the crossover from ballistic to diffusive transport.

Bibliography

[1] M. Voué and J. De Coninck. Spreading and wetting at the microscopic scale: recent developments and perspectives. *Acta Materialia*, pages 4405 – 4417, December 2000.

[2] T. B. Jones, M. Gunji, M. Washizu, and M. J. Feldman. Dielectrophoretic liquid actuation and nanodroplet formation. *Journal of Applied Physics*, 89(2):1441–1448, January 2001.

[3] A. I. Milchev and A. A. Milchev. Wetting behavior of nanodroplets: The limits of young's rule validity. *Europhysics Letters (EPL)*, 56(5):695–701, 2001.

[4] J. Yaneva, A. Milchev, and K. Binder. Polymer droplets on substrates with striped surface domains: molecular dynamics simulations of equilibrium structure and liquid bridge rupture. *J. Phys.: Condens. Matter*, 17(49):S4199–S4211, December 2005.

[5] H. Kusumaatmaja, J. Léopoldès, A. Dupuis, and J. M. Yeomans. Drop dynamics on chemically patterned surfaces. *Europhysics Letters (EPL)*, 73(5):740–746, March 2006.

[6] Michael Urbakh, Joseph Klafter, Delphine Gourdon, and Jacob Israelachvili. The nonlinear nature of friction. *Nature*, 430:525–528, July 2004.

[7] J. A. Nieminen, D. B. Abraham, M. Karttunen, and K. Kaski. Molecular dynamics of a microscopic droplet on solid surface. *Phys. Rev. Lett.*, 69(1):124–127, July 1992.

[8] Ju-xing Yang, Joel Koplik, and Jayanth R. Banavar. Terraced spreading of simple liquids on solid surfaces. *Phys. Rev. A*, 46(12):7738–7749, December 1992.

[9] J. De Coninck, S. Hoorelbeke, M. P. Valignat, and A. M. Cazabat. Effective microscopic model for the dynamics of spreading. *Phys. Rev. E*, 48(6):4549–4555, December 1993.

[10] P. G. de Gennes. Wetting: statics and dynamics. *Rev. Mod. Phys.*, 57(3):827–863, July 1985.

[11] M. Haataja, J. A. Nieminen, and T. Ala-Nissila. Molecular ordering of precursor films during spreading of tiny liquid droplets. *Phys. Rev. E*, 52(3):R2165–R2167, September 1995.

[12] S. F. Burlatsky, G. Oshanin, A. M. Cazabat, M. Moreau, and W. P. Reinhardt. Spreading of a thin wetting film: Microscopic approach. *Phys. Rev. E*, 54(4):3832–3845, October 1996.

[13] S. Bekink, S. Karaborni, G. Verbist, and K. Esselink. Simulating the spreading of a drop in the terraced wetting regime. *Phys. Rev. Lett.*, 76(20):3766–3769, May 1996.

[14] F. Heslot, N. Fraysse, and A. M. Cazabat. Molecular layering in the spreading of wetting liquid drops. *Nature*, 338:640, 1989.

[15] F. Heslot, A. M. Cazabat, P. Levinson, and N. Fraysse. Experiments on wetting on the scale of nanometers: Influence of the surface energy. *Phys. Rev. Lett.*, 65(5):599–602, July 1990.

[16] M.J. de Ruijter, T.D. Blake, and J. De Coninck. Dynamic wetting studied by molecular modeling simulations of droplet spreading. *Langmuir*, 15:7836 – 7847, October 1999.

[17] Chun Huh and L. E. Scriven. Hydrodynamic model of steady movement of a solid/liquid/fluid contact line. *Journal of Colloid and Interface Science*, 35:85 – 101, January 1971.

[18] V. E Dussan and S. Davis. On the motion of a fluid-fluid interface along a solid surface. *J. Fluid Mech.*, 65:71–95, 1974.

[19] Ju-xing Yang, Joel Koplik, and Jayanth R. Banavar. Molecular dynamics of drop spreading on a solid surface. *Phys. Rev. Lett.*, 67(25):3539–3542, December 1991.

[20] F. Heslot, A. M. Cazabat, and P. Levinson. Dynamics of wetting of tiny drops: Ellipsometric study of the late stages of spreading. *Phys. Rev. Lett.*, 62(11):1286–1289, March 1989.

[21] F. Tiberg and A.-M. Cazabat. Self-assembly and spreading of non-ionic trisiloxane surfactants. *Europhysics Letters (EPL)*, 25:205–210, 1994.

[22] A. M. Cazabat, J. De Coninck, S. Hoorelbeke, M. P. Valignat, and S. Villette. Influence of substrate heterogeneities on the spreading of a drop. *Phys. Rev. E*, 49(5):4149–4153, May 1994.

[23] S. F. Burlatsky, J. G. Berberian, J. Shore, and W. P. Reinhardt. Spreading of a macroscopic lattice gas. *Phys. Rev. E*, 54(2):1489–1496, August 1996.

[24] Douglas B. Abraham, Rodolfo Cuerno, and Esteban Moro. Microscopic model for thin film spreading. *Phys. Rev. Lett.*, 88(20):206101, May 2002.

[25] W. B. Hardy. The spreading of fluids on glass. *Philosophical Magazines*, 38:49–55, 1919.

[26] P. Brunet, J. Eggers, and R. D. Deegan. Vibration-induced climbing of drops. *Physical Review Letters*, 99(14):144501, 2007.

[27] A. B. Bortz, M. H. Kalos, and J. L. Lebowitz. A new algortihm for monte carlo simulation of ising spin systems. *Journal of Computational Physics*, 17:10, 1975.

[28] A. M. Cazabat. How does a droplet spread? *Contemp. Phys.*, 28(4):347 – 364, July 1987.

[29] Philip Ball. Spreading it about. *Nature*, 338:624 – 625, April 1989.

[30] L Leger and J F Joanny. Liquid spreading. *Reports on Progress in Physics*, 55(4):431 – 486, 1992.

[31] Mikel L. Forcada and C. Mathew Mate. Molecular layering during evaporation of ultrathin liquid films. *Nature*, 363:527 – 529, June 1993.

[32] David Landau and Kurt Binder. *A Guide to Monte Carlo Simulations in Statistical Physics*. Cambridge University Press, New York, NY, USA, 2005.

[33] M. E. J. Newman and G. T. Barkema. *Monte Carlo Methods in Statistical Physics*. Oxford University Press, USA, March 1999.

[34] Lars Onsager. Crystal statistics. i. a two-dimensional model with an order-disorder transition. *Phys. Rev.*, 65(3-4):117–149, February 1944.

[35] Bruria Kaufman. Crystal statistics. ii. partition function evaluated by spinor analysis. *Phys. Rev.*, 76(8):1232–1243, October 1949.

[36] T. D. Schultz, D. C. Mattis, and E. H. Lieb. Two-dimensional ising model as a soluble problem of many fermions. *Rev. Mod. Phys.*, 36(3):856–871, July 1964.

[37] K. Kawasaki. *Phase Transitions and Critical Phenomena*, volume 2. Academic Press, London, 1972. Edited by C. Domb and M. S. Green.

[38] J. Hoshen and R. Kopelman. Percolation and cluster distribution. i. cluster multiple labeling technique and critical concentration algorithm. *Phys. Rev. B*, 14(8):3438–3445, October 1976.

[39] M. E. Fisher. *Critical Phenomena.* Academic Press, London, 1971. ed. M. S. Green.

[40] V. Privman, C. Hohenberg, and A. Aharony. *Phase Transitions and Critical Phenomena*, volume 14. Academic Press, London, 1991. eds. C. Domb and J. L. Lebowitz.

[41] K. Binder. *Computational Methods in Field Theory.* Springer, Berlin, 1992. eds. C. B. Lang and H. Gausterer.

[42] Makoto Matsumoto and Takuji Nishimura. Mersenne twister: a 623-dimensionally equidistributed uniform pseudo-random number generator. *ACM Trans. Model. Comput. Simul.*, 8(1):3–30, 1998.

[43] T. D. Blake, A. Clarke, J. De Coninck, M. de Ruijter, and M. Voué. Droplet spreading: a microscopic approach. *Colloids and Surfaces A: Physicochemical and Engineering Aspects*, 149:123 – 130, April 1999.

[44] K. Binder and J.-S. Wang. Finite-size effects at critical points with anisotropic correlations: Phenomenological scaling theory and monte carlo simulations. *Journal of Statistical Physics*, 55(1-2):87–126, April 1989.

[45] J.-S. Wang, K. Binder, and J. L. Lebowitz. Computer simulation of driven diffusive systems with exchanges. *Journal of Statistical Physics*, 56(5-6):783–819, September 1989.